Magneto-transverse Phonon Transport

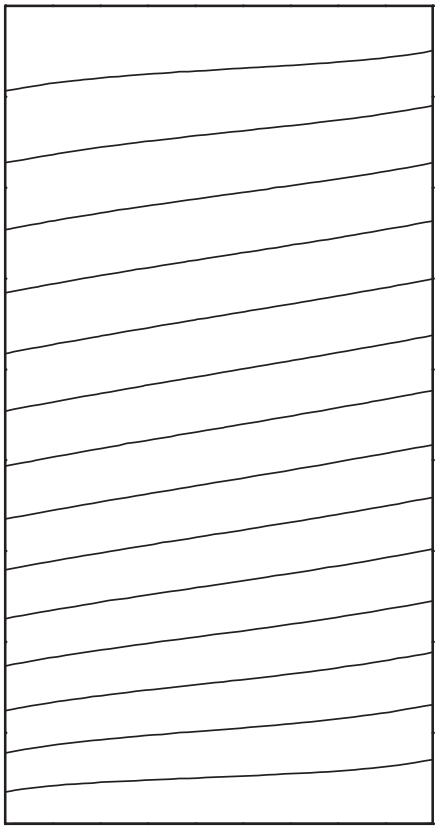

Dissertation zur Erlangung des akademischen Grades
eines Doktors der Naturwissenschaften
an der Universität Konstanz
Fachbereich Physik

vorgelegt von Cornelius Strohm

Tag der mündlichen Prüfung: 10. September 2003

Referent: Prof. Dr. Peter Wyder
Referent: Prof. Dr. Günter Schatz

Contents

List of Figures

Chapter 1

Introduction

1.1 Magneto-transverse thermal conductivity

In the classical Hall-effect [Hal79] a magnetic field induces a transverse voltage perpendicular to the original current direction and the magnetic field (fig 1.1 a)). The origin of this effect is the breaking of the time reversal symmetry by an external magnetic field through the Lorentz force. A similar effect was observed by Righi and Leduc [Led87] in the thermal conductivity of metals. A magnetic field induces a transverse temperature difference perpendicular to the original heat current and the magnetic field (fig 1.1 b)). This effect is due to the electronic contribution to the thermal conductivity of metals.

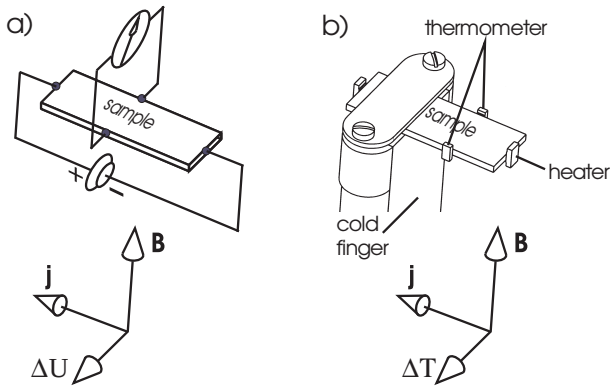

Figure 1.1: *Geometry of magneto-transverse transport effects. a): classical Hall-effect. b) Righi-Leduc effect, Senftleben-Beenakker-effect (the gas is contained in a sample cell) and magneto-transverse phonon transport.*

Hermans et al. reported a magneto-transverse thermal conductivity of paramagnetic gases [Her67] known as Senftleben-Beenakker-effect. The effect is due to an anisotropic scattering cross-section of the diffusing gas molecules responsible for the transport of heat. Rikken and Tiggelen [Rik96] observed the magneto-transverse diffusion of light in Faraday-active, multiple scattering samples. The magnetic field breaks the time reversal symmetry in polarized photon propagation and leads to an anisotropic scattering cross-section in multiple scattering.

As for the case of the photon diffusion, at first sight no such effect is expected for the phonon thermal conductivity, as there is no net charge associated with phonon transport. But phonons describe the collective motion of particles carrying charge and spin. A magnetic field splits the branches of the diamagnetic [Vin85] and paramagnetic [Tuc80] phonon dispersion relations and leads to the acoustic Faraday-effect.

To our knowledge no magneto-transverse effect for the phonon thermal conductivity has been reported yet in the scientific literature. We have investigated the magneto-transverse phonon transport in diamagnetic samples in [Str00] however without a conclusive result. In this thesis we experimentally investigated the magneto-transverse phonon transport of strongly scattering paramagnetic $Tb_3Ga_5O_{12}$ and found phenomenological evidence for the existence of a phonon analog to the classical Hall-effect and the Righi-Leduc-effect. We think that the microscopic realization is similar to the magneto-transverse diffusion of light.

1.2 Outline

After the introduction and the outline the thesis is subdivided in three main chapters. Theory, experiment and results, followed by a conclusion in English and German.

In the theory chapter we appreciate the existence of magneto-transverse phonon transport from a thermodynamic point of view, introducing the Onsager-relations before discussing the phenomenology of the effect. We then stress the analogy between phonons and photons for which the corresponding effect was modeled, to point out a possible microscopic realization of the effect. After a short review of the lattice dynamics in presence of a magnetic field we treat the thermal conductivity in terms of phonon gas. We finally state conditions for a successful experimental search for the effect.

In the Experimental part we present the equipment, methods and protocols used for the measurement of the longitudinal and transverse thermal conductivity as a function of temperature and magnetic field.

In the Results chapter we present the results obtained on samples of Terbium-Gallium-Garnet ($Tb_3Ga_5O_{12}$) and discuss the significance of the data.

Chapter 2

Theory

We first discuss the possible existence of magneto-transverse phonon transport from a thermodynamic point of view, without going into details concerning the microscopic realization of the effect. There is no theory on the magneto-transverse thermal conductivity in dielectric solids yet. After an analysis of the phenomenology we therefore stress the analogy to photons for which a transverse effect has been observed and theoretically described. We present a simple model for the optical case. We shortly review the lattice dynamics and the thermal conductivity of dielectrics in order to show, where the magnetic field comes into play and to derive useful relations for the choice of samples and the interpretation of the results.

2.1 Symmetry considerations

Many transport phenomena can be described by phenomenological laws in which a current is linearly related to a potential gradient. Examples are Ohm's law for the electrical conduction, Fick's law for ordinary diffusion and Fourier's law for the case of thermal conductivity:

$$j_i = -k_{ij}\frac{\partial T}{\partial x_j} \tag{2.1}$$

k_{ij} is called the thermal conductivity tensor and relates the heat current j to the originating gradient $\partial T/T\partial x_j$. The tensor character reflects the fact that heat conduction is not necessarily isotropic, i.e. the heat current arising from an applied temperature gradient depends on the orientation of the system. Furthermore the thermal conductivity tensor might contain an antisymmetric part. This means, that a temperature drop along one direction of the sample could be at the origin of a so called transverse heat current perpendicular to this direction.

Onsager investigated the symmetry properties of k_{ij} [1] in the framework of a general theory of the thermodynamics of irreversible processes [On31-1, On31-2]. His approach

[1] In his theory, Onsager is dealing with generalized fluxes and forces. The application to the different phenomena like thermal conduction is not straightforward. The case of the thermal conductivity has been treated by Casimir [Cas45].

was, that even if a process -like diffusion- is irreversible on a macroscopic scale, the microscopic motions should be reversible i.e. symmetric with respect to the reversal of time. In his theory he drew the symmetry of k_{ij} back to the symmetry of the microscopic equations of motion, however without the need to state them explicitly. He found:

$$k_{ij} = k_{ji} \tag{2.2}$$

In the same way it was then possible to predict the symmetry of $k_{ij}(B)$ of a system subject to a magnetic field B. In order to trace back the microscopic trajectories of motion in the presence of an external magnetic field, the field has to be reversed too when time is reversed. Onsager therefore concluded:

$$k_{ij}(B) = k_{ji}(-B) \tag{2.3}$$

This explicitly means, that k_{ij} is always symmetric for $B = 0$, but may contain an antisymmetric (transverse) contribution in the presence of a magnetic field. One further can conclude that any transverse effect is necessarily of odd symmetry with respect to B and that any longitudinal effect is necessarily of even symmetry with respect to the magnetic field [2].

A point of considerable importance is the geometry of these effects: The microscopic origin for the breaking of the time reversal symmetry (whether in electrical conductivity, anisotropic scattering in the diffusion of gases or the phonon thermal conductivity) is always the Lorentz-force. In consequence antisymmetric contributions occur only in a plane perpendicular to the magnetic field.

In the above paragraph we focused on the case of the thermal conductivity. The result is also valid for ordinary diffusion and electrical conductivity.

In our experiments we measure the longitudinal conductivity of temperature dependent resistors in order to detect a magneto-transverse temperature difference. These resistors are also magnetic field dependent. We make extensive use of the Onsager relations in order to reveal a field odd magneto-transverse temperature difference and to rule out any field even contribution due to the thermometer's longitudinal magnetoresistance which must be even according to eq. 2.3.

2.2 Phenomenology

Above we presented Fourier's law as a local relation between the temperature gradient $\partial T/\partial x_i$ and the heat current j_i arising from this current.

$$j_i = -k_{ij}\frac{\partial T}{\partial x_j} \tag{2.4}$$

We then argued from a thermodynamic point of view, that the thermal conductivity tensor k_{ij} may contain an antisymmetric contribution in the presence of an external

[2] This statement implicitly assumes that the system under consideration is invariant to parity reversal. Otherwise new effects arise [Rik01].

magnetic field. This leads to a heat current perpendicular to the original gradient and the magnetic field. However the heat current itself is experimentally not observable, but it is possible to probe the temperature distribution in the system.

For a given geometry of the system, the temperature distribution is the solution of the stationary heat equation

$$k_{ij}\frac{\partial}{\partial x_i}\frac{\partial}{\partial x_j}T = 0 \tag{2.5}$$

which is related to the Fourier law by the continuity-equation. To solve this partial differential equation, the boundary conditions need to be specified. On its boundary Γ the system may either be in contact with a reservoir R, maintaining the temperature at $f_D(\Gamma)$ (Dirichlet-condition):

$$T|_\Gamma = f_D(\Gamma) \tag{2.6}$$

Or the system is isolated or somehow exchanging energy with other systems as for example a thermometer probing the local temperature. In this case, the energy flow $f_N(\Gamma)$ across the boundary Γ is given by the Fourier-law

$$\left(k_{ij}\frac{\partial}{\partial x_j}T\right)\Bigg|_\Gamma n_i = f_N(\Gamma) \tag{2.7}$$

where n_i is the unit normal to the boundary (von Neumann-condition). On the thermally insulated boundaries, $f_N(\Gamma)$ is taken to be zero.

The heat equation may be solved analytically for special cases. Here, we have chosen a numerical approach. The case of a rectangular bar-shaped sample is equivalent to the case of a two-dimensional rectangular plate. We therefore will restrict our analysis to this situation. The surface is covered with an equidistant cartesian grid on which the heat-equation was linearized and solved numerically. Figure 2.1 shows the isotherms for a sample which is in contact with thermal reservoirs at different temperatures on the left and the right hand side in order to establish a thermal gradient. The other sides of the sample are assumed to be thermally insulated. In fig. 2.1 a) there is no antisymmetric contribution to the thermal conductivity tensor and the isotherms are parallel with respect to the sides in contact with the reservoirs. The temperature difference between opposite points on the upper and the lower side of the sample shown in fig. 2.1 b) is of course zero as any two opposite points are relied by an isotherm. In fig. 2.1 c) an antisymmetric contribution has been assumed. The isotherms are now inclined by an angle α with respect to the sides in contact with the reservoirs. Opposite points on the upper and the lower side of the sample are no longer relied by isotherms, a transverse temperature difference appears (fig. 2.1 d)). For an infinitely long sample the angle α equals the so-called Hall-angle:

$$\alpha = atan\left(\frac{k_{12}}{k_{11}}\right) \tag{2.8}$$

The phenomenology of the magneto-transverse thermal conductivity is in complete analogy with the classical Hall-effect, as the Heat-equation and the Poisson-equation are equivalent, if the potentials T and U and the conductivities k_{ij} and σ_{ij} were interchanged.

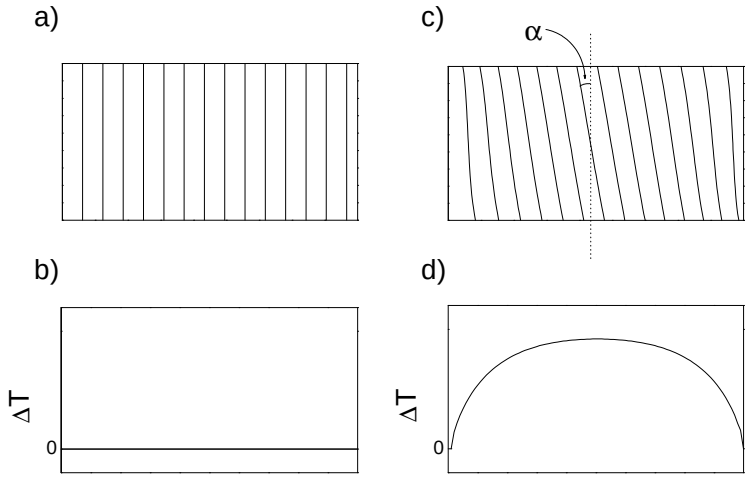

Figure 2.1: *Simulation of the isotherms in a rectangular bar-shaped sample. Heat is flowing from left to right. The longitudinal temperature difference between the hot side and the cold side is 5 K. The distance between the isotherms is 1/3 K. a): $k_{xy}/k_{xx} = 0$ b) No temperature difference appears between opposite sides of the sample. c)$k_{xy}/k_{xx} = 1/5$ The isotherms are now inclined by the so-called Hall-angle with respect to the hot and the cold side of the sample. d) Now a transverse temperature difference appears.*

2.3 Models and analogies

2.3.1 Phonons and photons

There are very far-reaching analogies in the propagation of photons and phonons. For example the Rayleigh scattering at structural details that are small compared with the wavelength. Photons as well as phonons show the characteristic dipole pattern that arises from the scalar product of the polarization vectors. The frequency dependence is proportional to ω^4 in both cases.

An other important point is the rotation of the polarization of a linearly polarized wave traversing a medium subject to a magnetic field parallel to the wave-vector $\mathbf{k}$, the Faraday-effect. Here even the orders of magnitude are comparable. But there are also important differences in the behaviour of photons due to the different characteristic length-scales that are involved:

If the wavelengths of photons and phonons were compared with the typical inter-atomic spacing of the structure in which they propagate it turns out that this ratio can be 2 in the case of phonons whereas it is of the order of 1000 for light in the visible spectrum. For phonons this leads to the effect of phonon focusing, whereas light can be described by an ellipsoid of refraction (Photon focusing in periodic dielectric structures has not been proposed till some years ago! [Etc96]). With regard to the cross-section model this could mean that small changes in the differential cross-section would perhaps not be detectable, because the anisotropy might be reduced by the focusing effect.

A very important difference is the fact that electromagnetic waves can propagate in the vacuum, whereas phonons have to be considered as a displacement field that is only unambiguously defined on lattice vectors. This in turn leads to the phenomenon of umklapp scattering, making phonon transport intrinsically diffusive, even in large and pure crystals. In the first experiments on the magneto-transverse diffusion of photons, the only scattering mechanism was the scattering at Faraday active particles. In phonon transport one has to go to low temperatures in order to make this the dominating process.

2.3.2 A simple model

In the case that the mean free path is much smaller than the size of the sample, the transport of photons can be described by a diffusion law, just like ohmic transport of electrons or thermal conduction:

$$j_i = -D_{ij}\frac{\partial \rho}{\partial x_j} \tag{2.9}$$

Here the photon current density per unit area is linearly related to the local photon density gradient by D_{ij}.

In 1995 B. van Tiggelen pointed out [Tig95], that D_{ij} may contain an antisymmetric contribution in presence of an external magnetic field. He calculated the magneto-transverse diffusivity $D_\perp$ for the case of a matrix containing randomly distributed

Faraday active Rayleigh-scattering particles:

$$D_{\perp}(B) = c_0 \cdot \frac{4m}{(m^2-1)(m^2+2)} \frac{VB}{k^2} \tag{2.10}$$

Where c_0 denotes the speed of light in vacuum, m the contrast in the refractive index of the matrix and the scattering particles, V the Verdet constant and k the wave-vector. This relation only holds true for the opaque regime.

An experimental observation of the effect was soon reported by G. Rikken [Rik96][3]. He measured the difference of the light scattered in opposite directions perpendicular to both the magnetic field and the incident light beam for rare earth compounds in glycerol. The field was modulated and the intensity difference was evaluated by means of a lock in amplifier. As signature for the effect the dependence on the sign and magnitude of the Verdet constant and on the volume fraction have been verified. The relative intensity changes due to the effect were found to be in the order of $10^{-5}\mathrm{T}^{-1}$.

Since then a lot of work has been done on the subject. We want to mention the observation of the magneto-transverse diffusion of light in so-called inverted media [Düc00]. In inverted media the effective Verdet constant of the medium is much bigger than of the scattering particles. This is very similar to the situation expected for the phonon case. Experimentally the following relation for the relative changes in the intensity has been confirmed:

$$\frac{\Delta I_{\perp}}{I_{\perp}} \approx BV_{eff}l^* \tag{2.11}$$

$$V_{eff} = V_s \cdot f_s + V_m \cdot f_m \tag{2.12}$$

with f_i and V_i being the volume fractions and the Verdet constants for the scattering particles and the matrix respectively and l^* the transport mean free path. A rigorous theoretical explanation for the inverted effect is however lacking till now. But the characteristic behaviour as well as the order of magnitude are described by eq. 2.11 and 2.12.

Equation 2.10 is the only rigorous equation derived so far that describes the magneto-transverse transport of classical waves. It does however not provide us with an intuitive picture of the underlying physics. In [Rik97] a simple model has therefore been developed for the case of Rayleigh scattering particles. We start with the dipole radiation pattern, that is typical for the case of Rayleigh scattering (fig 2.2). In presence of an external magnetic field this dipole pattern is distorted by an angle that can be shown to be proportional to the Verdet constant and B. However there is no anisotropy in the differential cross-section if the total intensity radiated to the top and to the bottom side were considered. The differential cross-section shows point symmetry around the axis of the magnetic field. If two scattering particles with a fixed phase difference were considered and the interference between the re-radiated waves is taken into account, an anisotropy in the forward and backward radiated intensity is

[3]This work is often referred to as "photonic Hall-effect". To the author's personal opinion, this is not appropriate. In the Hall-effect the transverse current is balanced by a transverse potential difference. The occurrence of this temperature difference is considered as the characteristic property of the phenomenon. In the optical case the relative intensity difference and thus the current is measured.

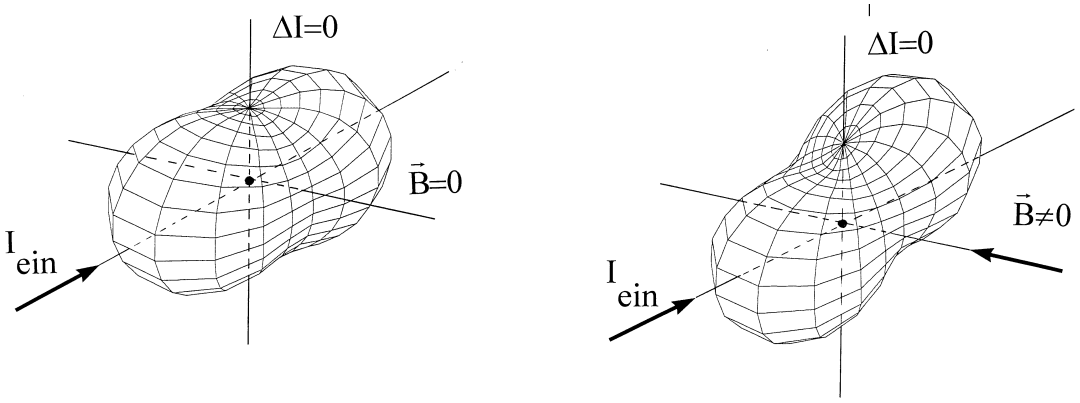

Figure 2.2: *Scattering cross-section for one scattering particle without and with magnetic field. [Rik97] Figures: courtesy of A. Sparenberg. I_{ein} denotes the incident light intensity.*

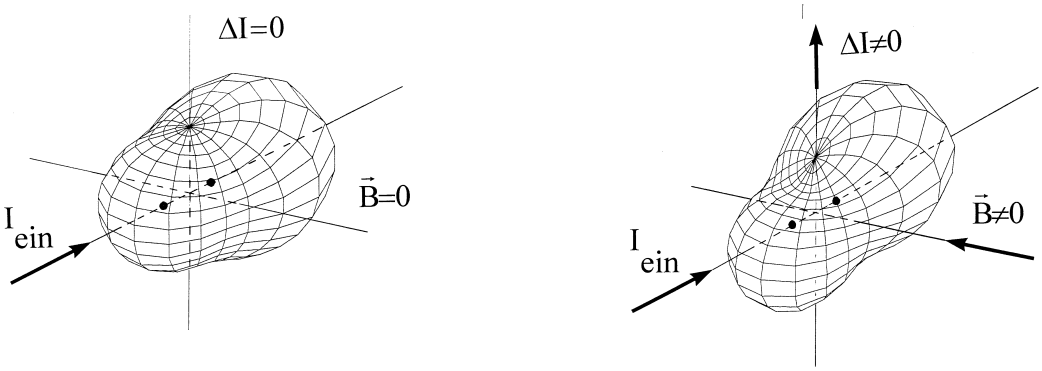

Figure 2.3: *Scattering cross-section for two scattering particles without and with magnetic field. [Rik97] Figures: courtesy of A. Sparenberg. I_{ein} denotes the incident light intensity.*

appearing, that finally leads to a transverse intensity difference if a magnetic field is applied (fig. 2.3).

2.4 Thermal conductivity

2.4.1 Lattice dynamics

In this section we discuss the vibrational motion of the ions in an ionic crystal. The magnetic field is included in the equations. In a magnetic field, the frequencies of the eigenmodes are perturbed with the perturbation parameter ω_c/ω, where ω_c is the ion cyclotron frequency and ω the phonon frequency. The eigenmodes turn out to be of elliptic polarization. For the propagation along directions of high symmetry the eigenmodes become circularly polarized. Therefore degenerate modes that were previously linear polarized are split up in left an right circular polarized modes with

different phase velocities. This leads to the so-called acoustic Faraday-effect. Important work on the subject has been done by [Vin85] and [Ana72].

To set up the equations of motion for the ions we denote the lattice vectors with $\mathbf{r}$. The positions of the ions in the basis with respect to the origin of the unit cell be $\mathbf{l}$. The deviation of the ion at $\mathbf{l}$ in the unit cell from its (classical) equilibrium position $\mathbf{r}+\mathbf{l}$ is designed by $\mathbf{u}(\mathbf{r}+\mathbf{l})$. The equations of motion can now be written in matrix notation, including the magnetic field:

$$M(\mathbf{r}+\mathbf{l})\ddot{\mathbf{u}}(\mathbf{r}+\mathbf{l}) = \sum_{\mathbf{r}',\mathbf{l}'} \mathbf{D}\left((\mathbf{r}+\mathbf{l})-(\mathbf{r}'+\mathbf{l}')\right)\mathbf{u}(\mathbf{r}'+\mathbf{l}') + \mathbf{F_L}(\mathbf{r}+\mathbf{l}) \tag{2.13}$$

Where $\mathbf{D}\left((\mathbf{r}+\mathbf{l})-(\mathbf{r}'+\mathbf{l}')\right)$ is the matrix of force constants and $\mathbf{F_L} = q\left(\dot{\mathbf{u}}(\mathbf{r}+\mathbf{l})\times B\right)$ the Lorentz force. This represents an equation system of $d\cdot N\cdot L$ coupled equations, with N the number of unit cells, L the number of atoms in the basis and d the number of space coordinates. For the diagonalization of this system of equations one assumes nearest neighbor interactions only. (The harmonic approximation has been made implicitly in the definition of $\mathbf{D}$.) We assume the solutions of this equations to be of the form:

$$\mathbf{u}(\mathbf{r}+\mathbf{l},t) = \hat{\mathbf{e}}\cdot e^{i(\mathbf{kr}-\omega t)} \tag{2.14}$$

with the polarization vectors $\hat{\mathbf{e}}$. The solutions are required to fulfill periodic Born von Karman boundary conditions. Inserting these solutions in the equations of motion, we get the three dimensional eigenvalue problem

$$\omega^2\hat{\mathbf{e}} = \mathbf{D}(\mathbf{k})\hat{\mathbf{e}} \tag{2.15}$$

with the mass weighted dynamical matrix:

$$\mathbf{D}(\mathbf{k}) = \sum_{\mathbf{r}} \mathbf{D}(\mathbf{r}+\mathbf{l})e^{i\mathbf{kr}} \tag{2.16}$$

In presence of a magnetic field the dynamical matrix contains now additional off diagonal elements of the form: $i\omega\omega_c$. The i results from the first time derivative of the u's. The eigenvalues stay nevertheless real, because the matrix is hermitian. The equation system has exactly one solution if the determinant

$$\det\left|\mathbf{D}(\mathbf{k}) - \omega^2\cdot\mathbf{1}\right| = 0 \tag{2.17}$$

vanishes. The expression for $\omega(\mathbf{k})$ for which the determinant vanishes is called the dispersion relation. For a d-dimensional lattice with a basis of L atoms, the general expression contains $(d\cdot L)!$ terms. Except for special cases this can only be evaluated numerically. Reinserting the ω's in eq. 2.15 yields the unit polarization vectors for the different modes. The Eigenmodes are now elliptically polarized because the Lorentz force couples the force on an ion in one direction to its velocity perpendicular to this direction and the applied magnetic field. To demonstrate the influence of the magnetic field on the Lattice vibrations we present in fig. 2.4 the dispersion relation for a two dimensional non centrosymmetric lattice of oppositely charged ions with a magnetic field perpendicular to the lattice. The dispersion relation has been calculated using an

expression given in [Vin85]. At $B = 0$ the two acoustic and optic modes are degenerate. This degeneracy is lifted through the application of a magnetic field. The splitting at fixed k is linear in the applied field. If one calculates the velocity of sound $v_s = \omega/k$ it turns out, that the changes for the left and right hand circular modes are proportional to $\pm\omega_c/\omega$. This has an interesting consequence: A transverse polarized wave can be described by to counter-rotating circularly polarized waves. In a magnetic field they have different velocities and in consequence they acquire a phase difference ϕ per unit length

$$\phi \sim \omega \left(\frac{1}{v_s^{\sigma-}} - \frac{1}{v_s^{\sigma+}} \right) \tag{2.18}$$

which in turn can be interpreted as a rotation of the plane of polarization of the original linear polarized wave. The rotation angle in radians per unit field and length is called the Verdet constant. This effect is in complete analogy with the optical Faraday-effect.

For crystals with NaCl structure, Rikken [Rik96-2] has derived the Verdet constant for acoustic phonons propagating along the (100) directions:

$$V \approx \frac{-q\ \omega^3 (m_2 - m_1)}{32\ k_0^2\ a} \quad [V] = \frac{\text{rad}}{\text{T m}} \tag{2.19}$$

Where q is the ionic charge, ω the phonon frequency, m_1 the masses of the positively and m_2 of the negatively charged ions, k_0 the force constant and a the lattice constant. The sign of the Verdet constant depends on whether the positively or the negatively charged ion is heavier. In fig. 2.5 we calculated the Verdet constants for the alkali halides with the sodium chloride structure [Str00]. For this purpose eq. 2.19 was frequency averaged, weighted with a Planck distribution for 4.2 K. The lattice constants and the force constants have been taken from [Hak79]. The force constants were averaged. For a given alkali ion the force constants decrease from Fluorine to Iodine. The highest acoustic Verdet constants among the alkali halides are thus expected to be those of NaI and KI.

In a quantum mechanical description the equations of motion are diagonalized by the introduction by quasiparticles called phonons. The state of the lattice is then described by the number of phonons $n_{\omega,\sigma}$ in the normal mode with frequency ω and polarization σ. Anharmonic contributions and interactions are then included as scattering processes causing transitions from one state to another.

2.4.2 Phonon scattering

In this section we will briefly address the scattering of phonons from impurities and the resonant scattering of phonons from two level systems.

Rayleigh scattering

Mass difference scattering occurs from isotopic impurities, i.e. from lattice sites where the atom, originally of mass M has been replaced by an atom of mass $M + \Delta M$. The Hamiltonian of the system consists of a sum of kinetic- and potential- energy

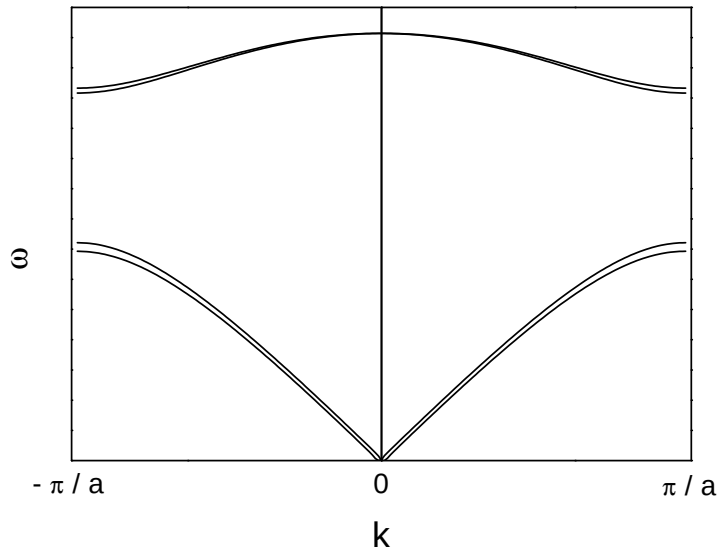

Figure 2.4: *Dispersion relation for a two dimensional lattice with two atoms in the basis in a magnetic field. The graph was calculated using an expression given in [Vin85]. A splitting in the previously degenerate acoustic and optic modes becomes visible. This causes a change in the phase velocities and finally leads to the the Faraday-effect. The graph was taken from [Str00]*

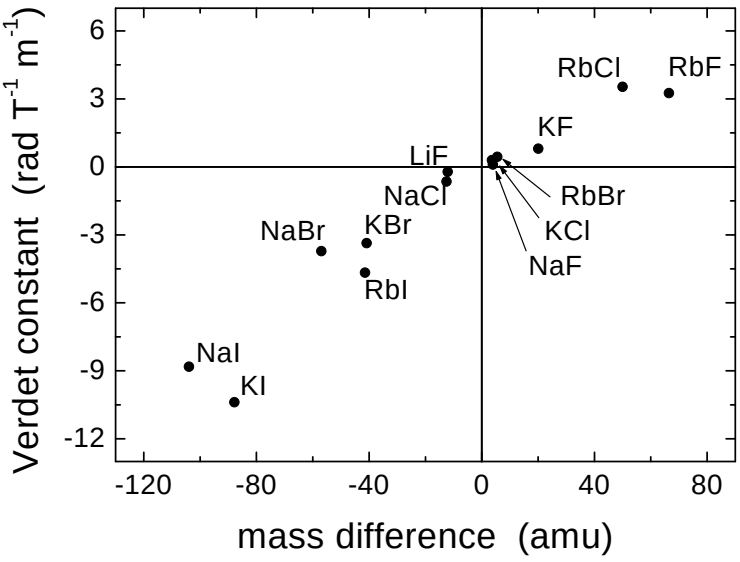

Figure 2.5: *The frequency averaged Verdet-constant weighted with a Planck distribution for 4.2 K. This quantity is not accessible to measurement, but allows to classify sample systems.*

terms for each atom. One of the kinetic energy terms of the Hamiltonian is then perturbed by $H' = (p^2/2M) \cdot (\Delta M/M)$. The local change in the force constants is neglected. The perturbation induces transitions between originally independent states. Klemens [Kle55] calculated the resulting transition rate in first order time dependent perturbation theory,

$$\tau^{-1} = \frac{2\pi}{\hbar} \sum_f |\langle f|H'|i\rangle|^2 \delta(\omega_i - \omega_f) \tag{2.20}$$

where the initial $|i\rangle$ and final $|f\rangle$ states of the unperturbed Hamiltonian were treated in the framework of the second quantization. His final result for the total scattering rate is:

$$\tau^{-1} = \frac{1}{4\pi N} \cdot \left(\frac{a}{v}\right)^3 \cdot \left(\frac{\Delta M}{M}\right)^2 \cdot \omega^4 \tag{2.21}$$

Here a is the lattice constant, ω the phonon frequency, N the number of atoms in the crystal and v Debye's weighted mean sound velocity for the three acoustic branches. To obtain this result, the k space sum has been converted into an integral making Debye's approximation of an isotropic dispersionless solid. The result shows the typical ω^4-dependence for Rayleigh scattering.

The differential scattering cross-section $\mathrm{d}\sigma/\mathrm{d}\Omega$ for the scattering of phonons by isotopes has been calculated by Weis [Wei95].

$$\frac{\mathrm{d}\sigma}{\mathrm{d}\Omega} = \frac{1}{4\pi v_i} \cdot \left(\frac{a}{v_f}\right)^3 \cdot \left(\frac{\Delta M}{M}\right)^2 \cdot \omega^4 \cdot \{\hat{\mathbf{e}}_i \cdot \hat{\mathbf{e}}_f\}^2 \tag{2.22}$$

The characteristic angular dependence results from the scalar product of the unit polarization vectors $\hat{\mathbf{e}}_i$ and $\hat{\mathbf{e}}_f$ for the incident and the outgoing phonons respectively, v_i and v_f denote the sound velocities for the phonons in the initial and in the final state. The resulting scattering characteristics are shown in fig. 2.6. The longitudinal polarizations have been labeled with D (dilatational), the two orthogonal transverse polarizations with S1 (shear) and S2. All patterns show rotational symmetry around the k-vector of the incident phonon. The cross-section for the scattering of transverse phonons is much bigger than for longitudinal phonons. This is due to the velocity v_f in the denominator of eq. 2.22. The sound velocity for longitudinal acoustic phonons is typically two times bigger than the velocity for the transverse phonons. For the same reason there is a high probability for longitudinal phonons to decay into transverse phonons, whereas the inverse is much less probable. This means that the transport of heat in samples with strong Rayleigh scattering is mainly due to transverse phonons.

The general result for the differential cross-section in an anisotropic solid is of considerable complexity [Wei95]. When replacing the sum in k-space in equation 2.20 by an integral over frequencies, without making the Debye approximation a term appears relating solid angles in k-space to solid angles in real space: $\mathrm{d}\Omega_k/\mathrm{d}\Omega_r$. This accounts for the anisotropic propagation of acoustic waves, know as phonon focusing, in the cross-section.

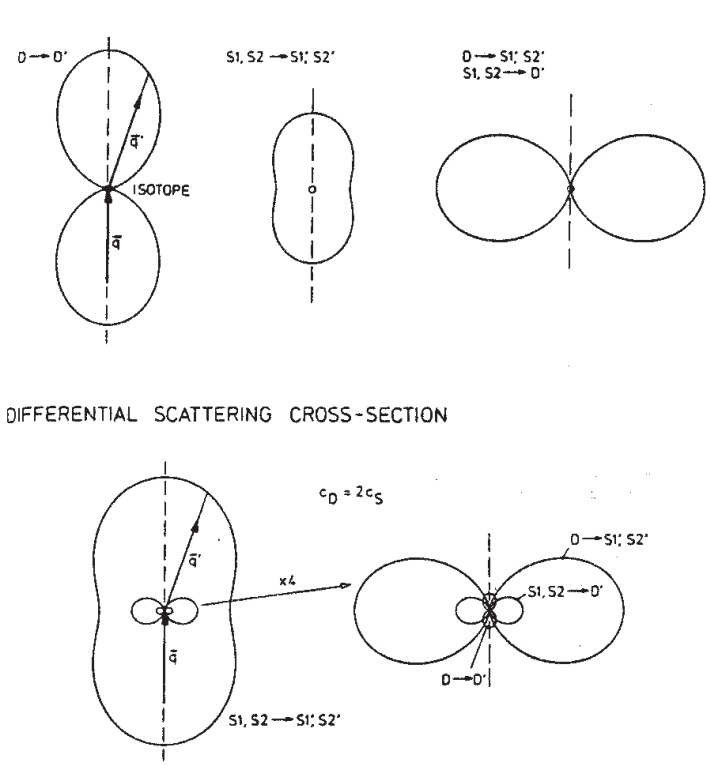

Figure 2.6: *Differential phonon scattering cross-sections. In the upper part the normalized contributions for the different polarizations of the incident and the outgoing phonons are shown. In the lower part they were combined to illustrate their relative contribution for a realistic case, where the ratio of the longitudinal sound velocity to the transverse sound velocity* $c_D/c_S = 2$*. The graph was taken from [Wei95].*

Resonant scattering

Phonons can induce electronic transitions when the phonon energy $\hbar\omega$ matches the energy splitting Δ between the involved levels. This is called resonant phonon scattering. In diamagnetic crystals containing paramagnetic ions and in pure paramagnetic crystals, phonons can be resonantly scattered by previously degenerate Zeeman levels, split by an applied magnetic field. This is referred to as spin-phonon-scattering.

In the case that the wavelength of the resonant phonons is equal or larger than the spacing of the paramagnetic ions (impurities), it is no longer possible to consider the lattice dynamics and the spin system independently. The correct description is then in terms of coupled spin-phonon modes. In the phonon dispersion relation, previously degenerate branches are then split with a pole at the resonant energy. It is not clear whether this coherent scattering - despite its finite lifetime - reduces the phonon thermal conductivity.

The problem of spin-phonon scattering has been treated by [Rou70] and [Tuc80] and reviewed with respect to the application to thermal conductivity data by [Nee72] and [Hof01].

The authors start with a Hamiltonian containing a phonon term and a Zeeman term and include the so called spin-phonon interaction term. Their main result is the calculation of a spin-phonon relaxation rate τ_{res}^{-1} that can directly be included in the integral (eq. 2.27) for the calculation of the thermal conductivity. They further calculated a dispersion relation for the coherent case. They argue that in the case of dilute randomly distributed paramagnetic impurities, the scattering due to the different ionic mass and due to the locally different force constants of the impurity $\tau_{\Delta M}^{-1}$ can be separated from the resonant spin-phonon scattering τ_{res}^{-1}:

$$\tau^{-1} = \tau_{\Delta m}^{-1} + \tau_{res}^{-1} \tag{2.23}$$

The relaxation rate $\tau_{\Delta M}^{-1}$ due to mass difference scattering has the form discussed in section 2.4.2. For the spin- phonon relaxation rate they give the following result:

$$\tau_{res}^{-1}(\omega, T) = C\frac{\omega^4\Delta^2}{(\omega^2 - \Delta^2)^2}F(T) \tag{2.24}$$

C is a phenomenological spin phonon coupling constant and $F(T)$ accounts for the (thermal) population of the levels involved in the scattering process. The result is valid for any two level system, that is linearly coupled to the phonons, not only for the spin-phonon interaction. There are no results on the differential scattering cross-section in a magnetic field.

In fig. 2.7 the dispersion relation for low energy acoustic phonons is shown. The previously degenerate linear dispersion branch is now split with a pole at the resonant frequency. This splitting then leads to an acoustic analog of the (optical) Faraday-effect in paramagnetic crystals. It is however not easily possible to define a Verdet constant as it has been done for the diamagnetic case, because the magnetic field does not only linearly change the splitting of the dispersion relation but shifts at the same time the resonance. (In the optical case, the Zeeman energy is always negligible with respect to the photon energy of the transition).

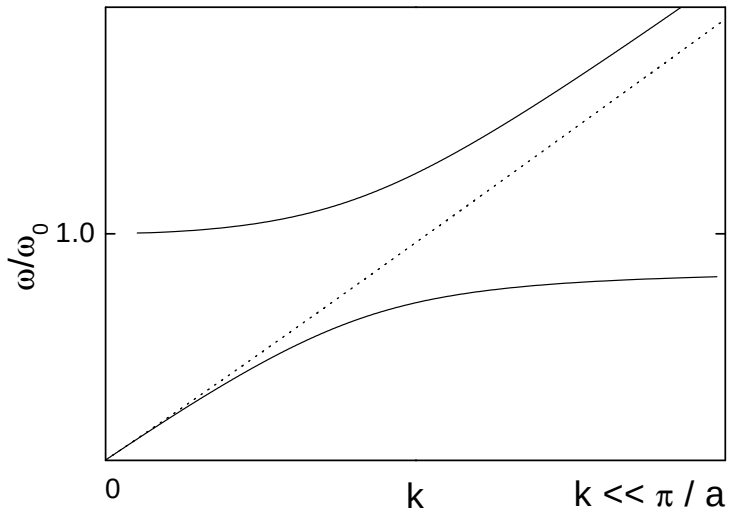

Figure 2.7: *Dispersion relation for a paramagnetic crystal subject to a magnetic field. The previously degenerate acoustic modes are split with a pole at the resonant frequency* $\omega_0 = \Delta_Z/\hbar$ *. At every frequency, the system responds with tow different k vectors, leading to an acoustic analog of the optical Faraday-effect. The graph was calculated using a relation given in [Tuc80].*

2.4.3 Thermal conductivity

In section 2.4.1 the microscopic motions of the ions in a dielectric solid have been discussed. It has been mentioned that the theoretical description becomes far less complicated if these equations were decoupled introducing quasiparticles called phonons. The anharmonicity of the potential, the ambiguity of the phonon wave-vector and interactions had been included in this picture in terms of phonon scattering. The parameters that characterized the system were thus frequencies, occupation numbers and relaxation times. In this chapter we are going to describe the transport of heat in the thermodynamic sense. In order to simplify the problem we treat the phonons in a simple kinetic model as a free phonon gas. We further assume the scattering processes to be independent from each other (Matthiessens rule). The remaining picture is the following [Cal58], [Haw70]:

The amount of energy flowing through a solid per unit time and cross-section j can be linearly related to the applied temperature gradient $\partial T/\partial x$.

$$j = -k \cdot \frac{\partial T}{\partial x} \tag{2.25}$$

The temperature dependent coefficient k is called the thermal conductivity and is calculated in the following way: Each phonon mode designed by its frequency ω and polarization state σ is contributing to the transport of energy depending on its occu-

pation number $n_{\omega,\sigma}(T)$ group velocity v and relaxation time $\tau_{\omega,\sigma}$.

$$k = \sum_{\omega,\sigma} \hbar\omega \; n_{\omega,\sigma}(T) \; v^2_{\omega,\sigma} \; \tau_{\omega,\sigma} \tag{2.26}$$

For evaluation the sum is converted into an integral using the Debye approximation for the density of states:

$$k = \frac{1}{2\pi^2 v} \int_0^{\omega_D} \frac{\hbar^2\omega^4}{kT^2} \frac{e^{\hbar\omega/k_BT}}{\left(e^{\hbar\omega/k_BT}-1\right)^2} \; \tau(\omega,T) \; \mathrm{d}\omega \tag{2.27}$$

The scattering processes limiting the phonon lifetimes are assumed to be independent. We therefore make a relaxation time approximation and calculate the reciprocal of the relaxation time as the sum of the reciprocals of the different contributions.

$$\tau^{-1}(\omega,T) = \sum_i \tau_i^{-1}(\omega,T) \tag{2.28}$$

After carrying out the integration over ω the thermal conductivity depends only on the temperature of the system.

The scattering of phonons from impurities and the resonant phonon scattering have been discussed in detail in section 2.4.2. In the following we summarize the different scattering processes that mainly determine the temperature dependence of the thermal conductivity at low temperatures.

Scattering processes

- boundary scattering:

$$\tau_b^{-1} = \frac{v}{1.12 \cdot L} \tag{2.29}$$

  Even in a perfectly harmonic crystal free from defects the phonon mean free path and therefore the thermal conductivity is limited by the (smallest) crystal dimension L. The 1.12 is a correction factor for quadratic sample cross-section.

- normal processes:

$$\tau_n^{-1}(\omega,T) = B_1\omega^2T^3 \tag{2.30}$$

  The normal processes account for the anharmonic perturbations in the Hamiltonian. In the phonon picture this corresponds to processes in which phonons scatter merge or decay according to the laws of energy and momentum conservation. The coefficient B_1 may be calculated theoretically but is normally adjusted to the experimental data.

- umklapp processes:

$$\tau_u^{-1}(\omega,T) = B_2\omega^2T^3e^{\frac{-\theta}{aT}} \tag{2.31}$$

As the temperature rises large phonon wave-vectors become involved and the resulting wave-vector of a phonon emerging from a collision may be larger than the first Brillouin-zone. In this case part of its momentum is carried over to the crystal reversing at the same time the direction of the outgoing phonon, much like in a reflection at the zone boundary. This is indeed the only process that would lead to a finite thermal conductivity, even in large and pure crystal. The calculation of B_2 and a is also possible but they are mostly fitted to the experimental data.

- mass difference scattering:

$$\tau_{\Delta m}^{-1}(\omega, T) = \frac{d^3}{4\pi v^3}\omega^4 \sum_i \left(\frac{m_i - m}{m_b}\right)^2 f_i \tag{2.32}$$

The mass difference scattering term accounts for scattering at substitutional isotopes and impurities with mass m_i. m is the average mass of the ion to be replaced by the impurity, m_b the mass of the basis and f_i the fractional concentration of the impurity with mass m_i. It is worth noting the Rayleigh-like ω^4-dependence. The differential cross-section for mass difference scattering has been discussed in chapter 2.4.2. Interstitial impurities lead also to the scattering of phonons, but the frequency-dependence is markedly different [Kle55].

- resonant scattering:

$$\tau_{res}^{-1}(\omega, T) = \sum_i C_i \frac{\omega^4 \Delta_i^2}{(\omega^2 - \Delta_i^2)^2} F_i(T) \tag{2.33}$$

Resonant phonon scattering at low-lying energy levels is possible, when the phonon energy $\hbar\omega$ matches the energy splitting Δ_i of the involved energy levels. C_i is a phenomenological coupling constant between the phonons and the i-th two level system and includes the concentration in the case of randomly distributed scatterers. $F_i(T)$ accounts for the (thermal) population of the energy levels.

For Zeeman-split levels, the energy splitting Δ_i is a function of magnetic field and introduces therefore a magnetic field dependence in the thermal conductivity. $F_i(T)$ also depends on B for energy levels that are shifted by a magnetic field. This thermal magnetoresistance however is only indirectly related to the antisymmetric contribution to k_{ij} which we are looking for in our experiments.

Experiments on the thermal conductivity as a function of temperature provide a good insight in the predominating microscopic scattering processes, by fitting the integral eq. 2.27 to the data.

It is perhaps worth noting, that such an experiment can be considered as broadband phonon spectroscopy: Except the boundary scattering, the processes all show a very marked frequency dependence. The spectrum of the phonons that are excited at a given temperature is given by a Planck-distribution. If the temperature is raised, the maximum of the Planck-distribution shifts linearly to higher frequencies with increasing temperature according to Wiens law. The transmission i.e. the thermal conductivity is then convolution of this (broadband) spectrum with the different scattering contributions.

2.5 Proposal for an experimental search for the magneto-transverse phonon transport

We are now going to resume the theory part in view of an experimental search for the effect. We will distinguish between phenomenological and thermodynamic arguments and arguments that are related to a special microscopic realization of the effect.

We argued, that from a thermodynamic point of view a magnetic field can induce an antisymmetric contribution to the thermal conductivity tensor. This leads to a heat current perpendicular to the incident current and the magnetic field. The antisymmetric contribution was shown to be an odd function of field. Furthermore it is expected from the Fourier law, that the transverse current arising from this contribution will be linear in the longitudinal gradient.

The heat current itself is not an observable quantity, but the induced changes in temperature. The temperature distribution is given through the solution of the heat equation with the appropriate boundary conditions. In a confined geometry no transverse currents are possible and have therefore to be balanced by a transverse potential difference, i.e. a temperature difference. The situation is in complete analogy with the Righi-Leduc-effect and the classical Hall-effect. Simple considerations lead to the conclusion, that the transverse temperature difference is the bigger, the bigger the width of the sample is made for constant cross-section perpendicular to the incident current; the width to length ratio should however not be greater than unity.

We have shown, that an applied magnetic field affects the phonon dispersion relation. In diamagnetic samples previously degenerate phonon branches are split due to the different charge to mass ratio of the ions. In paramagnetic samples the resonant spin-phonon scattering additionally leads to coupled spin-phonon modes if the average distance of the paramagnetic ions is smaller than the wavelength of the resonant phonons. In the dispersion relation of the coupled modes the previously degenerate acoustic phonons branches are also split with a pole at the resonant phonon frequency. The lifting of the degeneracy in the dispersion relation leads to the occurrence of the so called acoustic Faraday-effect in both, diamagnetic and paramagnetic samples. The magnetic field also affects the resonant scattering of dilute paramagnetic ions by shifting the resonance.

In analogy with the observed magneto-transverse diffusion of light we suggest that magneto-transverse phonon transport should occur in Faraday active, scattering media. The Faraday-effect breaks the time reversal symmetry in the propagation of photons as well as of phonons. It is also known that the Verdet constant scales the rotation of the scattering cross-section for the case of Rayleigh scattering. In strongly scattering media this leads to a magneto-transverse anisotropy in the interference pattern of the re-radiated waves. We assume that the simple cross-section model applies also for the acoustic case. In consequence the effect is expected to be linear in field due to the dependence on the Verdet constant.

In contrast to the propagation of light, the transport of thermal energy is intrinsically diffusive, except at low temperatures. The ideas about a microscopic realization of a magneto-transverse thermal conductivity effect in dielectric solids (based on the simple model) rely on the assumption, that the transport mean free path is dominated

by Rayleigh scattering.

The sample for an experimental investigation of the magneto-transverse thermal conductivity must be an insulator, because the intrinsic phonon thermal conductivity can only unambiguously be observed if no conduction electrons are present. The sample should have a big Verdet constant. In diamagnetic systems this is the case if the mass difference between the ions is important. In paramagnetic systems this is the case if the spin phonon coupling constant is high. In order to make resonant scattering and Rayleigh scattering the dominant processes the sample will have to be doped with impurities and the experiments have to be carried out below the maximum in the phonon thermal conductivity, where these scattering processes will play a dominant role. This can be specified in measurements of the thermal conductivity as a function of temperature. Samples in which the thermal conductivity is limited by the lattice specific heat (and boundary scattering) exhibit the typical Debye behaviour proportional to the third power of the temperature. In the case of dominant Rayleigh and resonant scattering the conductivity lies significantly below the Debye value.

As thermometers small resistance thermometers with an activated hopping behaviour are good candidates because they are readily available and allow for high sensitivities. A differential measurement scheme based on Onsager's relations will allow to separate any field even contribution of the thermometers electrical magnetoresistance from the odd magneto-transverse phonon transport we are looking for.

An unambiguous observation of the phenomenology of the effect needs to verify, that the effect is odd in the magnetic field, linear in the original longitudinal gradient and that the effect vanishes for the field being parallel to the original longitudinal gradient.

A microscopic understanding needs an investigation of the dependence on the microscopic coupling parameters (i.e the ion mass difference in diamagnetic systems or the spin-phonon coupling for paramagnetic systems) as well as on the scattering mean free path. The coupling constant and the mean free path both depend on the temperature. So first insight could be gained by a measurement of the temperature dependence.

Chapter 3

Experiment

We are now going to describe the methods, setups and protocols used for the measurements of the thermal conductivity as a function of temperature and magnetic field. The need to perform these experiments at low temperatures has been discussed in the theory chapter. We therefore shortly introduce the cooling techniques, inserts and our magnet system. We then present the apparatus for the measurement of the thermal conductivity as a function of temperature and the longitudinal thermal conductivity as a function of magnetic field. We discuss a measurement principle using the Onsager relations to rule out magnetic field effects on the thermometers in order to reveal any magneto-transverse effect.

3.1 Cryogenic equipment

The measurements on the magneto-transverse thermal conductivity effect have been performed in a ^{4}He bath cryostat allowing operating temperatures from 1.5 K to 4.2 K. In the experiments on the thermal conductivity as a function of temperature, a much larger operating range from 1.5 K to 77 K was needed in order to gain spectroscopic information on the different phonon processes that are involved. This temperature range was covered with a dynamic flux cryostat, that could be inserted in a normal bath cryostat. All the experiments are based on the measurements of temperature differences resulting from a heat current in a well defined direction. The experiments have therefore been carried out in a high vacuum insert, to avoid losses due to heat flow through the sample surfaces.

3.1.1 ^{4}He bath cryostats

In bath cryostats one makes use of the low boiling temperature of ^{4}He which is at 4.2 K at ambient pressure. Lower temperatures can be achieved by reducing the vapor pressure through pumping the ^{4}He bath. The vapor pressure of ^{4}He increases exponentially with temperature. The minimum temperature that can be reached with this method is limited by the maximum pumping rate to values above 1 K. In this temperature range the temperature scale is defined by the vapor pressure of ^{4}He in the

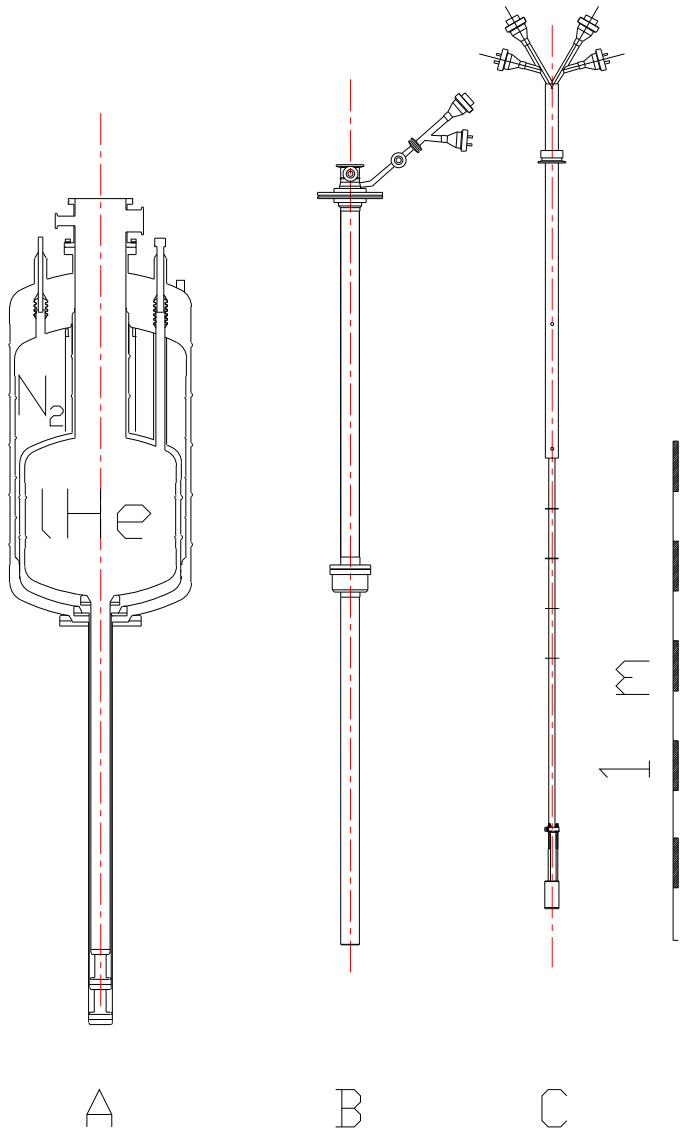

Figure 3.1: *A: ^{4}He bath cryostat. The tail of the cryostat fits in the 50 mm bores of the magnets. B: Dynamic flux cryostat that can be inserted in the ^{4}He bath cryostat. C: Insert (typical). The insert can either be inserted directly in the ^{4}He bath cryostat or be used in combination with the dynamic flux cryostat. Fig. courtesy of P. van der Linden*

ITS 90 temperature scale. For ^{4}He the latent heat of evaporation per volume is about thousand times smaller than for water. This means, that for an input power of 1 W roughly 1.4 l ^{4}He have to be evaporated per hour. In principle a cryostat is nothing else than a sophisticated vacuum jug. Convective transfer of heat is eliminated by the insulation vacuum. The heat load due to conduction is reduced through a long neck made out of thin stainless steel. Radiative input is kept small by a liquid nitrogen cooled radiation shield and by making the solid angles of all openings to the bath as small as possible. Figure 3.1 A shows a 20 l cryostat that has been used in the experiments. The peculiarity of the cryostats used in this laboratory is, that they are fitted with a tail that fits in the 50 mm bores of the resistive and superconducting magnets available in the laboratory.

3.1.2 Dynamic flux cryostat

Temperatures above 4.2 K can be reached with flux cryostats. The dynamic flux cryostat that has been used in the thermal conductivity measurements (fig 3.1 B) is inserted in a bath cryostat. The inner volume is thermally decoupled from the ^{4}He bath by a vacuum insulation. ^{4}He is aspirated from the bath through a thin capillary by pumping on the inner volume. The flow trough the capillary can be adjusted by a needle valve. At the bottom of the inner volume the ^{4}He is evaporated inside a sinter block. The insert with the experiment is placed in the inner volume and cooled by the cold gas stream. A heater and thermometers for different temperature ranges are placed on the sinter block in order to control the temperature of the gas stream. Temperatures below 4.2 K are reached by filling the inner volume through the capillary with liquid He. The needle valve is then closed and the temperature is decreased by pumping.

3.1.3 Insert

Similar inserts (fig. 3.1 C) have been used for the measurement of the thermal conductivity as a function of magnetic field and temperature. They mainly consist of a vacuum can supported by the pumping tube of stainless steel. Wiring has been made with very thin copper and manganin wires in order to reduce the heat load. For the measurement of the thermal conductivity as function of temperature a vacuum cell made out of brass has been used. Different sample holders can be connected to the cold plate inside this vacuum cell by a simple connector system. The cold plate and the corresponding surface on the sample holders are both made of high purity copper and were polished in order to reduce the thermal contact resistance. They were screwed together using brass screws. The differential thermal contraction warrants for a good contact. The vacuum can was sealed with silicone adhesive[1]. The seal proved to be reliable even below the λ-point but it does not withstand more than one cool-down to liquid He temperatures. The transmissions of the wires in the vacuum cell were sealed with epoxy [2] following standard techniques. For the measurement of the thermal conductivity as a function of magnetic field an insert with a plastic vacuum cell has been

[1] Rhone Poulenc: CAF 4
[2] EMERSON & CUMING: Stycast 2850 FT “black Stycast”

used. The cell is closed from the bottom with a cone seal plug. The experiments are mounted on these plugs which are fabricated with cable feedthroughs and thermal anchoring depending on the needs. We used vacuum grease [3] for the cone seal.

3.1.4 Magnet

An Oxford cryomagnetic system with a 50 mm room temperature bore has been used. The superconducting NbTi-coil reaches a maximum field of 10 T at 4.2 K. The sweep rate of this magnet is limited to 0.6 T per minute. The field polarity can be reversed. The magnet contains no switch. This offers the advantage, that the real current in the coil is known with better precision than in magnets containing a switch. The coil shows some remanence due to pinning, which has been measured to be of the order of 0.02 T. The knowledge of this value will be important for the analysis of the data on the transverse thermal conductivity.

The effect of the magneto-transverse thermal conductivity is expected to be linear in B, whereas the parasite effects like the magnetoresistance in the sensors are at least quadratic in field. The use of higher fields offers therefore no advantage.

3.2 Thermal conductivity as a function of Temperature

3.2.1 Method

For the measurement of the thermal conductivity as a function of temperature mainly three methods are used in a variety of different geometries: the steady state method, the AC method and the heat-pulse method. A further distinction is made between methods using an additional standard sample for determination of the incident heat current and methods where this current is directly calculated from the input power of the electric heater [Tou76]. We chose the steady state method for the ease of re-

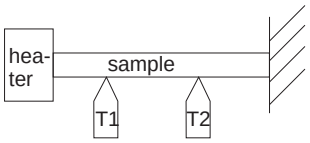

Figure 3.2: *The steady state method*

alization and straightforward interpretation of the results. In our setup we did not use an external standard. The sample holder is with many respect similar to apparatus described in [Sla57], [Kle66]. The rectangular bar-shaped sample is maintained at constant temperature at one side, whereas at the other end heat is supplied by an

[3] Rhone Poulenc: graisse pour vide

electrical heater (fig. 3.2). Probing the temperatures at two different positions along the sample between the hot and the cold side directly yields the thermal conductivity:

$$k(T_m) = \frac{l}{T_1 - T_2}\frac{P}{A} \qquad \text{with:} \qquad T_m = \frac{T_1 + T_2}{2} \tag{3.1}$$

Where P is the power supplied by the heater, A the sample cross-section and l the distance between the thermometers. The thermal conductivity is then plotted as a function of the mean sample temperature T_m

3.2.2 Sample holder

Figure 3.3 shows a rough sketch of the sample holder we employed for the thermal conductivity measurements. All thermal contacts to the sample are designed as spring loaded clamps with an interleave of thin indium foil enabling rapid changes of the samples, thermometers and heaters. Indium remains very soft, even at low temperatures. The interleaf therefore provides a good thermal contact, even if the sample surface is not perfectly flat. Furthermore it absorbs stress induced by the differential thermal contraction between the sample and the sample holder. This sample holder is mounted to the cold plate inside the vacuum can of the thermal conductivity insert.

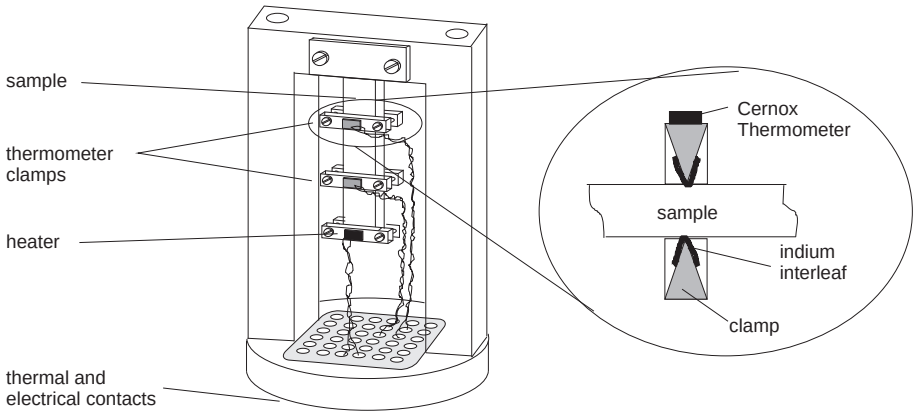

Figure 3.3: *The sample holder for the measurement of the thermal conductivity as a function of temperature.*

Thermometry As thermometers Cernox [4] bare chip resistors have been chosen for their characteristics enabling us to use a single set of thermometers over the whole operating range of the setup. The thermometers have been glued to the thermometer clamps with GE varnish [5]and were wired in four point configuration with 4 cm long manganin wires, 30μm in diameter. The current and voltage leads were twisted in order to reduce pickup. A third thermometer was placed on the sample holder in order to measure and stabilize the base-temperature. In the temperature range from 1.6 K

[4]Lakeshore Cryotronics: Cernox thermometers
[5]General Electrics: "GE varnish"

to 4.2 K they were calibrated against the vapor pressure of liquid ^{4}He. In the range from 4.2 K to 70 K the calibration was made against a ternary standard bought from Lakeshore Cryotronics. All relevant resistance values for calibration and measurement were read out with a self balancing ac resistance bridge [6] with $5\frac{1}{2}$ digits resolution, keeping the excitation current so small, that no self-heating could be detected. An additional multiplexer was used to switch between the resistances on the thermometer clamps and on the base. Data recording and the switching and self balancing procedure were controlled by a personal computer.

3.2.3 Experimental procedure

Each point in the thermal conductivity versus temperature plot was obtained in the following way:

1. First the base temperature was roughly adjusted by regulating the evaporation rate with the needle-valve at the cryostat and the diaphragm pressure regulator in the pumping group.

2. Then the temperature of the gas stream was further stabilized by regulating the heater power at the gas exit with a PID-controller [7] referencing either a Pt 100 or an Allen Bradley resistance mounted in the cryostat.

3. Finally the temperature at the cold plate inside the vacuum can has been maintained constant with a LR 130 temperature controller [8] using the resistance on the sample holder read out by a Barras precision resistance bridge [9] as reference. The final stability of the base temperature was better than 100μK at most temperatures.

4. The heater power at the sample was now adjusted at the current source such that the resulting temperature difference between the thermometer clamps was big enough to be detected with sufficient precision but nevertheless very small compared with the absolute temperature. For a precise determination of the heater power, the voltage drop was directly measured at the heater resistance.

5. For each point the temperatures T_1 and T_2 have been read out at least 50 times to ensure good statistics and to detect eventual drift in the mean sample temperature.

6. The thermal conductivity is then calculated according to equation 3.1 and plotted versus the mean sample temperature T_m. (A correction to account for the self-heating of the sensors and for the heat losses through the heater and thermometer wires seemed not necessary.)

[6] Linear Research: LR 700
[7] Barras Provence: Ohmmetre regulateur
[8] Linear Research: LR 130 PID controller
[9] Barras Provence: Pont de mesure & Detecteur Multifonction

3.3 Transverse thermal conductivity as a function of magnetic field

3.3.1 Method

The goal of the experiment is to measure the magneto-transverse thermal conductivity $k_{xy}(B)$. In a sample of finite geometry this leads to a transverse temperature difference $\Delta T_\perp$. The phenomenology of this effects has been discussed in section 2.2. The rectan-

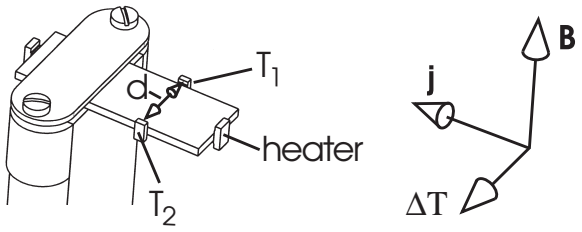

Figure 3.4: *Measurement of the magneto-transverse thermal conductivity.*

gular bar-shaped sample is placed in the magnet such that a temperature gradient can be established perpendicular to the magnetic field. This is done by thermal anchoring of the sample on one side, whereas at the other end heat is supplied from an electric heater. A set of thermometers R_1 and R_2 serves to probe the temperature difference in a direction perpendicular to both the magnetic field and the applied longitudinal gradient. The thermometers are temperature-dependent resistances. The design of the sample holder is very similar to apparatus for the measurement of the Righi-Leduc-effect described in the literature [Fle76]. The measurement principle however is somewhat different and the resolution has been increased. The transverse thermal conductivity is then evaluated as follows:

$$k_{xy}(T_m, B) = -\frac{T_1 - T_2}{d}\frac{A}{P}k_{xx}^2(T_m, B) \qquad \text{with:} \qquad T_m = \frac{T_1 + T_2}{2} \tag{3.2}$$

Where P is the power supplied by the heater, A the sample cross-section, d the sample width and T_m the mean sample temperature.

3.3.2 Measurement principle

In addition to the transverse conductivity there will be a change in the longitudinal thermal conductivity $k_{xx}(B)$ leading to a change in the longitudinal temperature gradient $\Delta T_{||}$. In order to measure the transverse temperature difference $\Delta T_\perp$, temperature dependent electrical resistors $R_1(T)$ and $R_2(T)$ are placed on opposite sides of the sample. As the magneto-transverse temperature difference is expected to be very small we measure the difference of the longitudinal electrical resistance $R_1(T) - R_2(T) = \Delta R(\Delta T)$ of these thermometers. The symmetry of the longitudinal and the transverse temperature difference as well as the resistance of the thermometers

behave according to Onsager's relations that we introduced in 2.1. The following table summarizes the behaviour of the sample and the resistors, when subject to a magnetic field:

parameter	symbol	Onsager rel.	character
magneto-transverse thermal conductivity	k_{xy}	$k_{xy}(B) = k_{yx}(-B)$	"odd"
longitudinal thermal conductivity	k_{xx}	$k_{xx}(B) = k_{xx}(-B)$	"even"
el. magnetoresistance of thermometer	ρ_{xx}	$\rho_{xx}(B) = \rho_{xx}(-B)$	"even"

If both thermometers were equal and placed perfectly symmetrically on the sample, the magnetoresistance would cancel out $\Delta R(B=0) = \Delta R(B) = 0$ and when sweeping the field any remaining ΔR could be attributed to a transverse temperature difference. But:

- different magnetoresistance and temperature dependence: $R_1(T,B) \neq R_2(T,B) \quad \forall \quad (T,B)$ so there will be a difference $\Delta R(B,T)$
- misalignment of the thermometers: the thermometers are not positioned perfectly symmetrically on the sample and therefore measuring a $\Delta T_{||}(B)$ due to the thermal magnetoresistance.

These two unwanted contributions can be ruled out if we make use of the symmetries of the involved effects. We therefore evaluate the magneto-transverse temperature difference $\Delta T_{\perp}^{ev}$ as follows: We first measure the difference $R_1 - R_2 = \Delta R$ for positive (ΔR_+) and reversed (ΔR_-) fields and subtract the latter from the first: $\Delta R_+ - \Delta R_-$. The transverse temperature difference is then obtained by dividing this difference by the mean sensitivity s_m of the thermometers. We now show that this protocol yields the "true" transverse difference and rules out field even contributions:

$$\Delta T_{\perp}^{ev} = \frac{1}{2s_m}\Big\{ \Big(R_1\big(+B, T + \frac{1}{2}\Delta T_{\perp}\big) - R_2\big(+B, T - \frac{1}{2}\Delta T_{\perp}\big)\Big) - \\ - \Big(R_1\big(-B, T - \frac{1}{2}\Delta T_{\perp}\big) - R_2\big(-B, T + \frac{1}{2}\Delta T_{\perp}\big)\Big)\Big\} \tag{3.3}$$

We use the symmetries $R(+B,T) = R(-B,T)$ and $\Delta T_{\perp}(B) = -\Delta T_{\perp}(-B)$. For small ΔT we can expand R_i around T: $R_i(T+\Delta T) = R_i(T) + s_i \Delta T + O(\Delta T^2)$ where s_i is the sensitivity in ΩK^{-1}. We finally obtain:

$$\Delta T_{\perp}^{ev} = \frac{1}{2s_m}\Delta T_{\perp}\Big(s_1 + s_2\Big) = \Delta T_{\perp} \tag{3.4}$$

Where $s_m = \frac{1}{2}(s_1 + s_2)$ defines the mean sensitivity. However, this procedure critically relies on two assumptions:

- temperature stability: The mean sample temperature does not change when sweeping the field from $+B$ to $-B$ and

- field precision: The absolute value of the magnetic field $+B$ precisely equals the absolute value of the magnetic field $-B$. This is nontrivial in superconducting coils due to flux pinning phenomena.

In the following we discuss 4 types of possible artifacts that may arise from insufficient temperature stability and field reproducibility.

Type 1: Temperature drift (+ different sensitivity to temperature)

We assume no transverse temperature difference to occur and we assume the mean sample temperature to change from T to $T+\Delta T$ while sweeping the field from positive to reversed direction:

$$\Delta T_{\perp}^{ev} = \frac{1}{2s_m}\Big\{ \Big(R_1(+B,T) - R_2(+B,T)\Big) - \\ - \Big(R_1(-B,T+\Delta T) - R_2(-B,T+\Delta T)\Big)\Big\} \tag{3.5}$$

We again make use of the symmetry of $\Delta T_{\perp}$ and R and expand $R(T)$ as above.

$$\Delta T_{\perp}^{ev} = -\frac{s_1 - s_2}{s_m}\Delta T \tag{3.6}$$

This means that a global temperature change of ΔT while reversing the field direction leads to the detection of an apparent temperature difference of ΔT^{ev}, scaled by the ratio of the sensitivity difference of the two resistance thermometers R_1 and R_2 to their mean sensitivity.

Type 2: Field imprecision (+ different sensitivity to temperature)

The sample is thermally anchored at one side whereas heat is supplied at the other side by a heater. The thermometers for the differential measurement are placed at a distance d from the heat sink at T_{base}. The mean sample temperature at the thermometers location is then determined by the temperature drop along the sample: $T_{mean} = T_{base} + \frac{j}{k_{xx}(B,T)}d$. If the magnetic field however assumes the value $-B + \Delta B$ instead of $-B$ after current reversal this leads to a change of the mean sample temperature of:

$$\Delta T_{mean} = jd\Big(\frac{1}{k_{xx}(B)} - \frac{1}{k_{xx}(B+\Delta B)}\Big) \approx \frac{jd}{k_{xx}(B,T)^2}\frac{\partial k_{xx}(B,T)}{\partial B}\Delta B \tag{3.7}$$

which in turn -due to "type 1"- will lead to the detection of an apparent transverse temperature difference:

$$\Delta T_{\perp}^{ev} \approx -\frac{jd}{k_{xx}(B,T)^2}\frac{\partial k_{xx}(B,T)}{\partial B}\Delta B\frac{s_1 - s_2}{s_m} \tag{3.8}$$

Type 3: Field imprecision (+ different magnetoresistance)

We again assume no transverse temperature difference to occur and we assume the field after current reversal to be $-B + \Delta B$ instead of $-B$.

$$\Delta T_{\perp}^{ev} = \frac{1}{2s_m}\Big\{ \Big(R_1(+B,T) - R_2(+B,T)\Big) - \\ - \Big(R_1(-B+\Delta B,T) - R_2(-B+\Delta B,T)\Big)\Big\} \tag{3.9}$$

Once again we use the symmetries of $\Delta T_{\perp}$ and of $R(B)$ and expand $R(T,B)$ around B as follows: $R_i(B+\Delta B) = R_i(B) + s_i \Delta B + O(\Delta B^2)$ where s_i^m is the sensitivity of R_i to B in units of ΩT^{-1}. We then obtain:

$$\Delta T_{\perp}^{ev} = -\frac{s_1^m - s_2^m}{s_m}\Delta B \tag{3.10}$$

This means that a field hysteresis (for example due to flux pinning) of ΔB leads to the detection of an apparent temperature difference which is scaled by the ratio of the difference in magnetic field sensitivity of the resistance thermometers R_1 and R_2 to their mean sensitivity.

Type 4: Field imprecision (+ misalignment of thermometers)

The idea to rule out contributions of the thermal magnetoresistance $k_{xx}(B)$ relies on the assumption that $|B| = |-B|$. If there is a misalignment δ of the thermometers they will be at different temperatures due to the longitudinal temperature gradient along the sample. The temperature difference is then: $\Delta T = \frac{j}{k_{xx}(B,T)}\delta$ Because of the thermal magnetoresistance, the longitudinal gradient changes as a function of magnetic field. This contribution is even in the magnetic field and cancels out in a differential measurement. If the magnetic field however assumes the value $-B + \Delta B$ instead of $-B$ after current reversal there remains an apparent temperature difference of:

$$\Delta T_{\perp}^{ev} \approx \frac{j\delta}{k_{xx}(B,T)^2}\frac{\partial k_{xx}(B,T)}{\partial B}\Delta B \tag{3.11}$$

3.3.3 Sample holder

Vacuum cell As magneto-transverse thermal conductivity effects are known to exist in metals due to the electronic contribution to the thermal conductivity, any metallic parts in the thermal pathway from the sample to the He bath have to be avoided. The whole vacuum cell is made out of Araldite [10] epoxy resin and is sealed with a plug featuring a greased cone seal. The experiment itself is mounted on this plug. In figure 3.5 the sample holder is shown. As thermal conductor between the sample and the He bath a high purity LiF single crystal has been used, providing reasonable thermal conductivity in the temperature range of the experiments on the TGG samples to be

[10] Bostik Sa.: Araldite

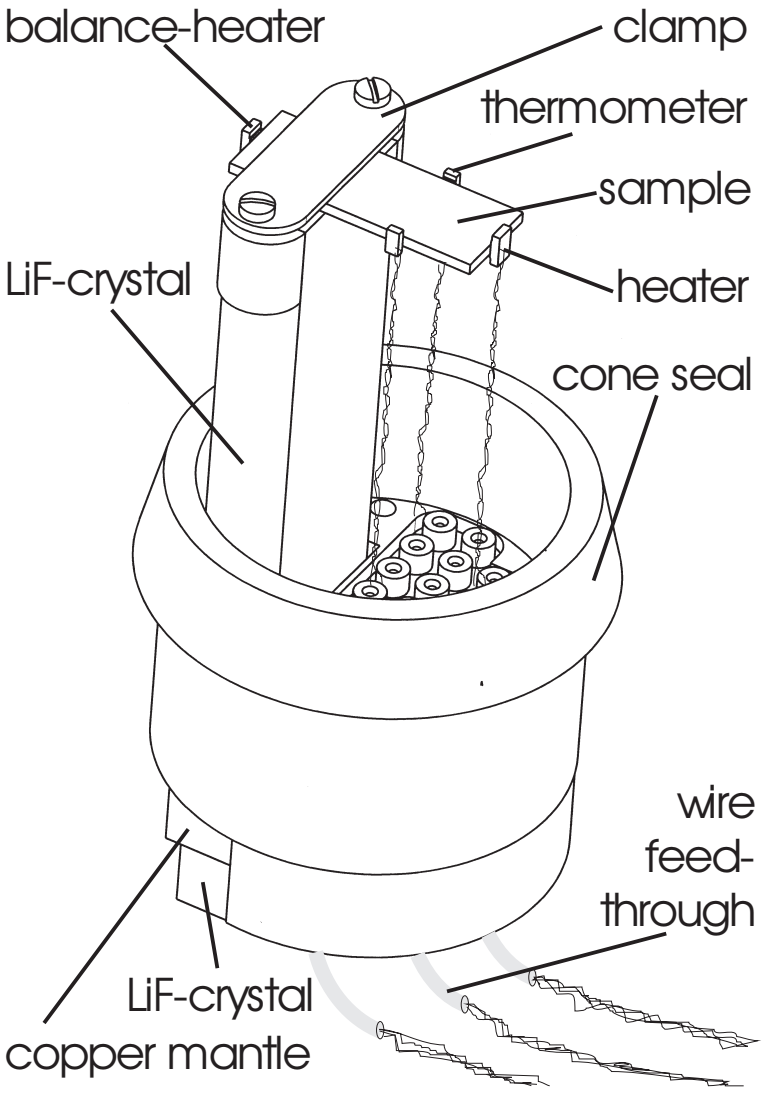

Figure 3.5: *The sample holder for the measurement of the magneto-transverse thermal conductivity. Drawing: H. Dresler.*

performed. The feedthrough of the LiF crystal from the vacuum space to the He-bath was realized by a very thin mantle of soft copper foil. The mantle serves to allow for the differential thermal expansion between the LiF crystal and the Araldite cone plug. The connections between the crystal and the copper at one side and between the copper and the Araldite cone at the other side have been glued with expansion matched epoxy resin. We emphasize that the copper mantle lies not in the thermal pathway and can furthermore be considered to be on an isothermal. The transmissions of the wires through the cone into the vacuum space have been sealed with epoxy too. The LiF crystal is equipped with a capacitive thermometer and a bifilar manganine heater to allow for field independent base temperature stabilization. Good temperature stability was obtained slightly above 4.2 K with a SMD chip capacitor sensor mounted on the LiF crystal (dielectric: KR 7) that was read out with an ultra high precision capacitance bridge [11] and a lock in amplifier [12]. The heater at the cold plate was driven by the output signal of the lock-in amplifier with a PID controller [13]. A point of considerable importance is the thermal anchoring of the sample at the cold side. In the interface between the sample and the sample holder there will always be a temperature drop due to the different sound velocities in the different materials, heat being only partially transmitted through the interface. The situation is much like for light that is reflected at a window. The acoustic analogues to the Fresnel formulae are treated in [Ana81]. Very useful numerical values for a great number of materials are calculated in [Che76]. These considerations however apply mainly to single crystals at very low temperatures. The most important result is, that the boundary resistance scales with T^{-3} and with the ratio of the sound velocities of the two materials. Engineering aids and numbers are given in [Swa88]. The sample is clamped to the LiF crystal with a flexible plastic bar ensuring evenly distributed pressure on the thermal contact. A thin film of GE-varnish or Apiezon grease between the sample and the LiF crystal ensures good thermal contact. The sample is equipped with heaters on both sides: a sample heater to establish a temperature gradient along the free end of the sample and an balance heater, which allows to keep the mean sample temperature constant for different sample heater powers without changing the base temperature. A further advantage of this additional heater is, that much less heater power is needed to achieve this goal as it makes use of the temperature drop across the sample - LiF crystal interface. Metal film chip resistors have mainly been used as heaters. They show only a moderate temperature dependence in resistance. In most cases they were wired in a four point configuration in order to be able to determine the power supplied to the sample. Great care has been taken to align the heater parallel to the direction of B in order to avoid galvano-thermomagnetic effects to occur in the heater and to influence the results. The sample is equipped with resistance thermometers on both sides for the differential measurement. All thermometers are glued to the sample with GE-Varnish.

Thermometry For the measurement of the longitudinal and the transverse temperature differences we made use of the temperature dependent resistance of RuO_x thick film chip resistors. They show a semiconductor behaviour. The resistance is expo-

[11] General Radio: 1616 capacitance bridge
[12] EG & G: model 5210
[13] Linear Research: LR 130

nentially decreasing with temperature. This behaviour is due to thermally activated hopping. The temperature dependent resistance $R(T)$ is described by a hopping-law.

$$R(T) = a \cdot e^{\left(\frac{b}{T}\right)^{\frac{1}{4}}} \tag{3.12}$$

Here a and b are parameters to be adjusted to fit the experimental calibration data. Depending on the type and source of the RuO_x resistances it was sometimes necessary to fit not only a and b but also the exponent or to add offset terms. The magnetic field dependence is a transport phenomenon and thus depends on the mesoscopic properties of the resistances as well as on their geometry. In practice it is not possible to give a closed expression for the magnetic field dependence of these resistances (figure 3.7 a)). The geometry of these sensors for example is influenced by the tuning process with which the resistances are trimmed to their nominal value at room temperature during the manufacturing process. The important consequence for their use as matched thermometers is, that even a nicely matched pair can show considerable differences in the magnetoresistance (figure 3.7 b)). This is one of the limiting factors for the final resolution of the differential measurements as will be explained later. For the magneto-transverse thermal conductivity measurements the resistances have been calibrated to a hopping law against the vapor pressure of the liquid helium bath. In contrast to the calibrations for the other thermal conductivity apparatus, where very precise absolute values were needed, rough calibrations were sufficient for this experiment. The evaluation of the highly sensitive difference measurements requires only the sensitivity. The base- and mean sample-temperatures nevertheless can be determined with sufficient precision. The calibration was therefore accomplished while slowly (quasi-static) pumping down the cryostat without stabilizing each point in the temperature. Temperatures above 4.2 K have been extrapolated without making errors too big for our purposes.

The absolute value of the sensitivity $S(T) = \partial R/\partial T$ is also exponentially increasing with decreasing temperature. The absolute thermometric resolution of the setup might at first sight seem to be determined only by the resolution of the resistance bridge and the sensitivity of the sensors. It is however limited due to the drift induced apparent transverse temperature difference (equ. 3.6). The difference in the magnetoresistance dictates the necessary dynamic range of the bridge and therefore limits the electronic resolution.

Bridge For the measurement of the difference between the resistances a Barras [14] precision resistance bridge has been used. The resistances were wired in four point configuration. The advantage of a compensated bridge circuit using a Lock-in-amplifier as null detector is to expand the dynamical range of the lock in amplifier on the small deviations from equilibrium. The Barras bridge can be equilibrated to 10^{-5} on every range by means of a resistance decade. The analog deviation signal has then been read out with a multimeter [15], providing further digits. Care has been taken to keep the self-heating small enough not to influence the measurement.

[14] Barras Provence: Pont de mesure & Detecteur Multifonction
[15] Keitley Instruments: Multimeter 2000

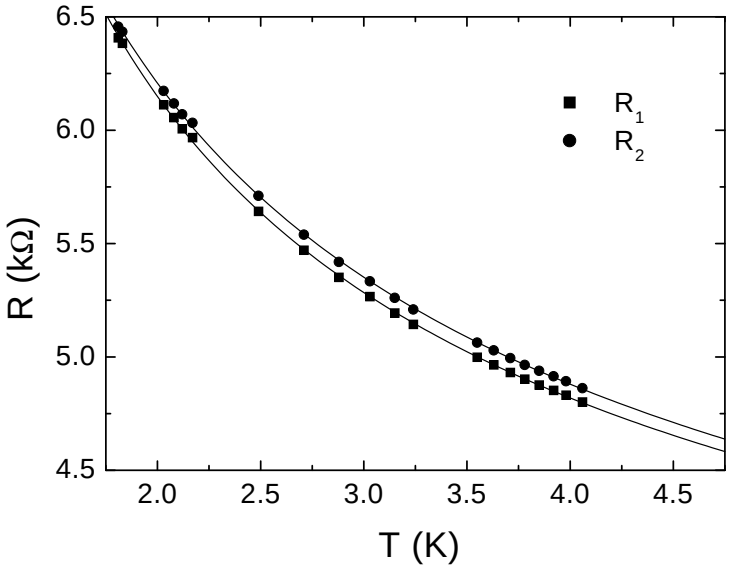

Figure 3.6: *Typical calibration curves for the transverse thermometers.(RuO_x)*

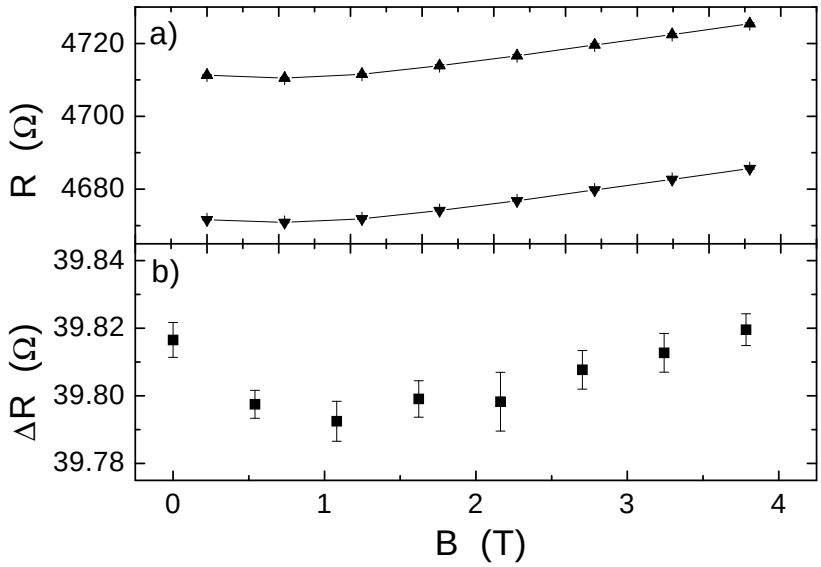

Figure 3.7: *a) Resistance R_1 (up triangles) and R_2 down triangles as a function of magnetic field. b) The difference $R_1 - R_2$ as a function of magnetic field measured with the differential bridge.*

3.3.4 Experimental procedure

In section 3.3.2 we discussed a differential measurement principle to measure the magneto-transverse temperature difference. The idea was to measure the difference of the temperature dependent resistances R_1 and R_2 for positive and reversed fields and to subtract the latter from the first in order to rule out even contributions like the magnetoresistance of the thermometers and the thermal magnetoresistance. We use the following protocol:

1. The base-temperature is stabilized in zero field using the capacitance thermometer on the LiF-crystal.

2. The sample heater power is set.

3. the balance heater is adjusted so as to realize the desired mean sample temperature.

4. The field is set to the desired value.

5. The differential bridge is equilibrated.

6. The resistance difference is now measured at positive field (fig. 3.8 a)).

7. The field direction is then reversed and the system is allowed to relax (magnetocaloric effect).

8. The resistance difference is now measured at reversed field.

9. The field is then swept back to the positive value.

10. The cycle 6. to 9. is now repeated as often as necessary, typically 3 to 4 times.

11. For each of these cycles the resistance differences at positive and reversed fields are then plotted in a cycle-graph An example is shown in fig. 3.8 b). A cycle consists of a measurement at positive and a measurement at reversed field direction. The lines connect the positive and reversed field values respectively. They are a measure of the overall drift while changing the field direction.

12. The measurements at negative fields are now subtracted from those at positive fields for each cycle. The difference is then averaged and converted to a temperature difference using the known mean sensitivity of the thermometers.

This procedure is repeated for every data point in a final graph (fig. 3.8 c))if not mentioned otherwise.

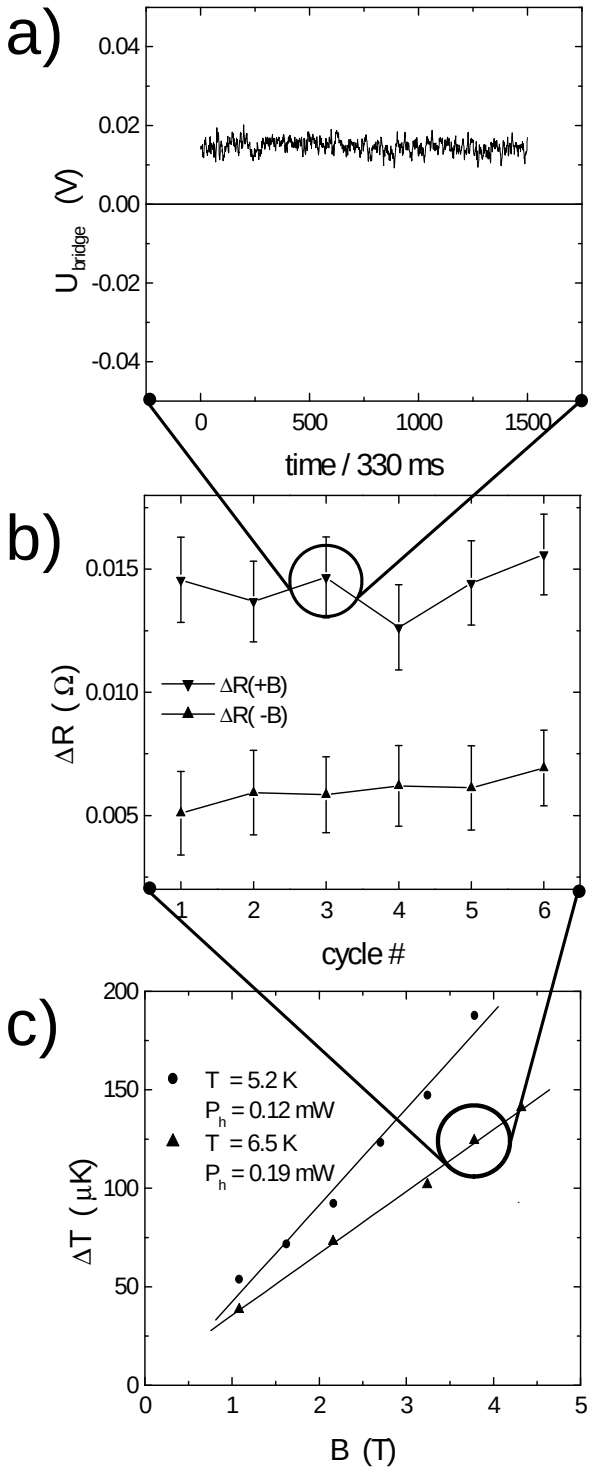

Figure 3.8: *The measurement procedure: a): Measurement of ΔR at positive field, roughly 8 minutes averaging time. b): Mean values of ΔR for positive and reversed field directions. The error bars result from averaging a). 6 cycles are shown. c): resulting temperature difference as a function of a parameter, here B.*

3.4 Longitudinal thermal conductivity as a function of magnetic field

3.4.1 Method

For the measurement of the longitudinal thermal conductivity k_{xx} as a function of B we use the same steady state method (fig. 3.9) as for the measurement of the thermal conductivity as a function of temperature. The data is evaluated as above, using eq.

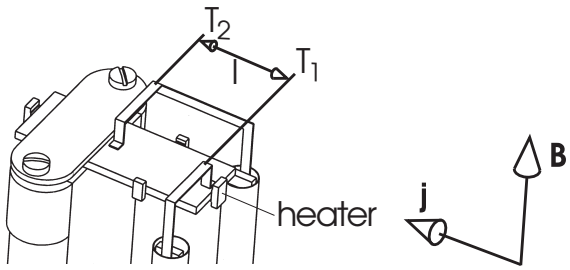

Figure 3.9: *Measurement of the longitudinal thermal conductivity as a function of B.*

3.2. But instead of plotting the data as a function of temperature they are now plotted as function of the magnetic field.

3.4.2 Sample holder

The sample holder for the measurement of the longitudinal thermal conductivity as a function of B is very similar to the one used for the measurement of the transverse thermal conductivity. For the measurement of the temperature drop along the sample we now additionally installed calibrated cernox hermetic package thermometers like the ones used for the measurement of the thermal conductivity as a function of temperature. For practical reasons however they are not mounted directly to the sample, but on small turrets with negligible thermal conductivity. The thermometers are thermally connected to the sample with thin sheets of silver foil. The turrets are hollow cylinders made out of a single layer of cigarette paper which is hardened with dilute standard household adhesive. The thermometers are contacted in four point configuration with twisted 30μm maganine wires. The wires are wound helicoidally around the turrets to make them as long as possible in order to reduce their thermal conductivity. The changes in the longitudinal thermal conductivity of the samples of TGG measured in this thesis are so big, that a correction of the thermometers for their (rather small: few percent) electrical magnetoresistance was not necessary. The sample holder is shown in figure 3.10. With this sample holder simultaneous measurements of the longitudinal and the transverse thermal conductivity are possible in principle, but have not been performed successfully yet.

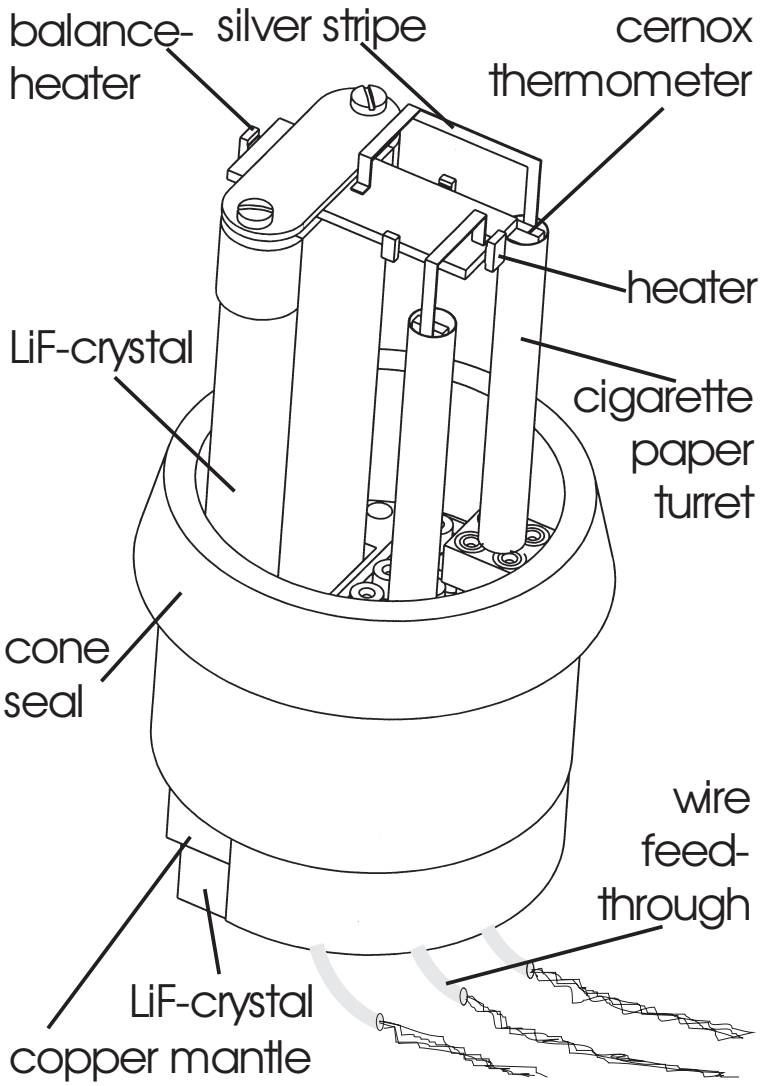

Figure 3.10: *The sample holder for the measurement of the longitudinal thermal conductivity as a function of B. This sample holder can in principle be used for simultaneous measurements of the longitudinal and the transverse thermal conductivity. Drawing: H. Dresler.*

3.4.3 Experimental procedure

The protocol for a measurement is the following:

1. The base-temperature is stabilized in zero field using the capacitance thermometer on the LiF-crystal.
2. The sample heater power is set.
3. The balance heater power is adjusted so as to realize the desired mean sample temperature if necessary.
4. The field is set to the desired value and the system is allowed to relax (magnetocaloric effect).
5. The bridge is balanced automatically and a parameter set is generated for the multiplexer system.
6. The temperatures of R_{hot}, R_{cold} and R_{base} are measured (automatically) several times, averaged and the thermal conductivity is calculated according to equation 3.1.

The steps 4 to 6 are repeated for every field value.

Chapter 4

Results

In the theory chapter we discussed the expected dependence of the magneto-transverse thermal conductivity on the Verdet constant and the transport mean free path. Insight in a possible microscopic realization of the effect could be gained in terms of a simple model for the optical case assuming Rayleigh scattering. The experimental techniques and setups were presented in detail in the preceding chapter. In this chapter we present measurements on the magneto-transverse thermal conductivity of $Tb_3Ga_5O_{12}$ (TGG) and discuss their significance.

4.1 Samples

The experiments presented in this thesis have been obtained on two single crystalline samples of TGG from different sources. The crystal structure is cubic with roughly 80 atoms per unit cell. For this reason there are a great number of optical phonon modes starting at low frequencies. The dispersion relation of these optical phonon modes is flat. Therefore they don't contribute much to the thermal conductivity and the thermal conductivity is mainly due to the three acoustic branches [Sla71]. One sample that will be referenced as TGG 1 in the following was cut from a crystal purchased beforehand from Gsaenger. The other sample was cut from a piece of TGG kindly given to us by FEE-Crystals. We will refer to this sample as TGG 2. Both samples were cut with a diamond blade and the surfaces were ground with fine sandpaper in order to reduce specular phonon reflection from the surfaces. The samples are not crystallographically oriented.

sample	dimensions	source
TGG 1	$1.114 \times 3.85 \times 25$ mm^3	Gsaenger
TGG 2	$0.67 \times 5.7 \times 17$ mm^3	FEE-Crystals

Both samples stem from suppliers of TGG for optical experiments and Faraday-isolators. They are normally interested in the highest possible amount of Terbium ions. For this reason Terbium is added in excess over the stoichiometric amount.

4.2 Thermal conductivity of TGG

We measured the thermal conductivity of TGG 1 using the apparatus described in section 3.4. In figure 4.1 we show our data together with data taken by [Sla71]. The data clearly can be subdivided into two distinct classes of different thermal conductivities. Both classes show the typical phonon peak, and a more or less pronounced dip which is attributed to resonant scattering. An analysis of the low temperature part of the data shows, that the thermal conductivities of all samples are strongly reduced with respect to the expected (phonon heat capacity limited) T^3-behaviour. The exponents of a fit to

$$k_{xx}(T) = a \cdot (T - b)^c \tag{4.1}$$

are listed in the table together with the respective lattice parameters. a, b and x are fit parameters. The difference between the two classes of crystals is attributed to non resonant phonon scattering at impurities, namely Terbium ions added over the stoichometric amount, occupying Gallium sites [Sla71]. This guess is supported by the fact that the lattice constant

sample	symbol	lattice parameter	$k_{xx} \propto T^c \quad c =$
R156	$\bigtriangledown$	12.3403 Å	1.64
R165	$\bigtriangleup$	12.3383 Å	1.76
R160	$\circ$	12.3476 Å	0.90
TGG 1	$\bullet$	unknown	0.82

is slightly higher for the low thermal conductivity curve of [Sla71]. For Gadolinium Gallium Garnet ($Gd_3Ga_5O_{12}$, GGG) no resonant scattering has been observed in measurements of the thermal conductivity. Gadolinium and Terbium have nearly the same mass and in GGG Gadolinium has nearly the same ion radius as Terbium in TGG. The lattice thermal conductivity of GGG and TGG should therefore be equal, if resonant scattering and impurities were absent in the latter. In fig. 4.1 we therefore also plotted the calculated thermal conductivity for pure GGG based on data given in [Nee72] for comparison.

In fig. 4.2 a), we show a level scheme proposed by [Gui85] for the six lowest energy levels of Terbium in TGG. It can be seen that there are a number of levels with a spacing at energies corresponding to the dip in the thermal conductivity. However, we did not succeed in a quantitative analysis of the data in fig. 4.1 using eq. 2.27. This is due to the lack of knowledge about the coupling of the phonons with the Terbium levels, the great number of transitions to consider and the influence of higher levels. Furthermore one has to account for the fact, that the substitutional Terbium ions on Gallium sites will have a different spectrum [Sla71]. This is illustrated in fig. 4.2 b), where the level scheme of Terbium is shown for different hosts.

Despite the lack of quantitative understanding, the data on the thermal conductivity allows nevertheless the important conclusion to be drawn, that the mean free path for the phonon transport is limited by impurity scattering and resonant scattering. Both are considered to be necessary conditions for the occurrence of a transverse thermal conductivity effect.

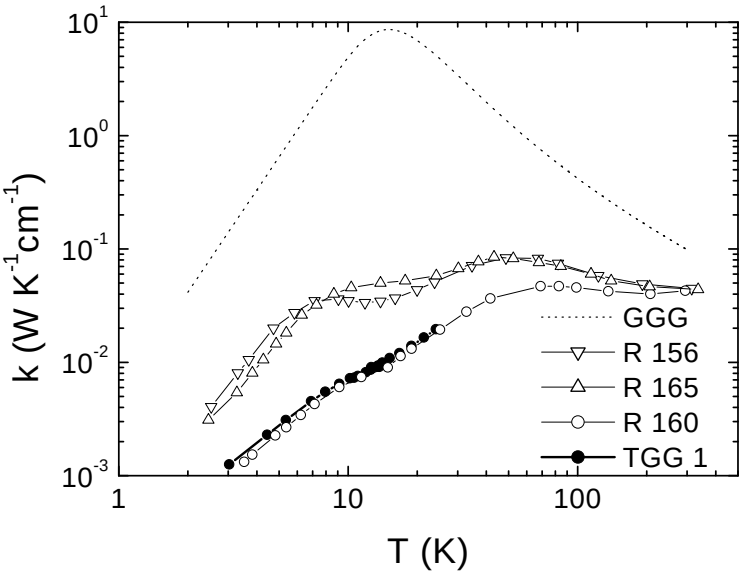

Figure 4.1: *The thermal conductivity of TGG as a function of temperature. Full circles: data taken on a piece of TGG from which sample TGG 1 was cut. Open symbols: Data taken from [Sla71]. The solid lines are only meant to guide the eye. Dashed line: calculated thermal conductivity of GGG.*

.

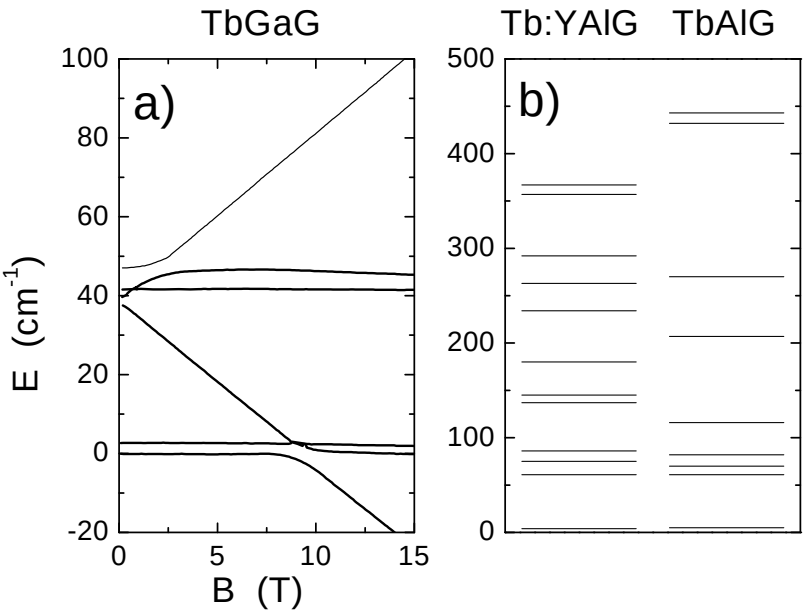

Figure 4.2: *a) level scheme for the lowest Tb-levels in TGG. The data was taken from [Gui85]. b) energy levels of TGG in different hosts. The data was taken from [Sla71].*

4.3 Thermal magnetoresistance

We measured the thermal conductivity of TGG 2 around 6 K as a function of magnetic field (fig. 4.3). In fig. 4.4 we also show a graph with the derivative of the thermal conductivity with respect to the magnetic field, as this will be of importance for the analysis of the data on the transverse thermal conductivity in section 4.5. The thermal conductivity shows a pronounced dip at 1 T. The obvious interpretation would be the resonance of the magnetic field split levels in fig. 4.2 a) with thermal energies or the crossing of the forth and the fifth level. As for the thermal conductivity data as a function of temperature we did however not succeed in a successful quantitative interpretation with the data that was available to us. But the data witnesses the Zeemann splitting which leads to the acoustic Faraday-effect due to spin-phonon scattering. In the framework of the simple model, the acoustic Faraday-effect is considered to be a necessary condition for the occurrence of a transverse thermal conductivity effect.

4.4 Transverse thermal conductivity

We performed measurements of the magneto-transverse temperature difference on the samples TGG 1 and TGG 2 using the apparatus presented in section 3.3.

TGG 1 Figure 4.5 shows the first data obtained on the sample TGG 1. Part of the data has been obtained using the full protocol described in section 3.3.4 for the rest only one cycle has been measured. It can be seen, that the transverse temperature difference is linear in B for low fields and that it depends on the mean sample temperature and the heater power. No systematic studies were made on this sample. However it has been verified, that the signal vanishes when the sample is oriented parallel to the magnetic field and that the signal is dependent on the originating heat current. We plot the transverse temperature difference and not the transverse conductivity, as this would need the knowledge of $k_{xx}(B)$ which has not been measured for TGG 1.

TGG 2 For all data presented here for sample TGG 2 the protocol (section 3.3.4) has been strictly followed and at least 4 full cycles have been measured. Figure 4.6 a) shows such a measurement. The values for the respective field directions nearly don't vary which confirms a good mean sample temperature stability. In a number of such measurements however it was observed, that the first measurement yields a value that is clearly distinct from the values obtained in further cycles (figure 4.6 b)). These jumps only occur in the first cycle after changing the field value or after a new cool-down of the sample holder. The error bar of the measurement is far too small to account for this behaviour. In rare cases this behaviour could be observed to be a sharp jump during the measurement of a data point. The problem is not yet understood. In the interpretation of the data we deliberately omitted the first cycles. We will show, that doing so yields a consistent data set. In sections 4.5 and 4.6 we will argue, that -to our knowledge- this behaviour could not account for the observation of the magneto-transverse thermal conductivity by misinterpretation of an artifact.

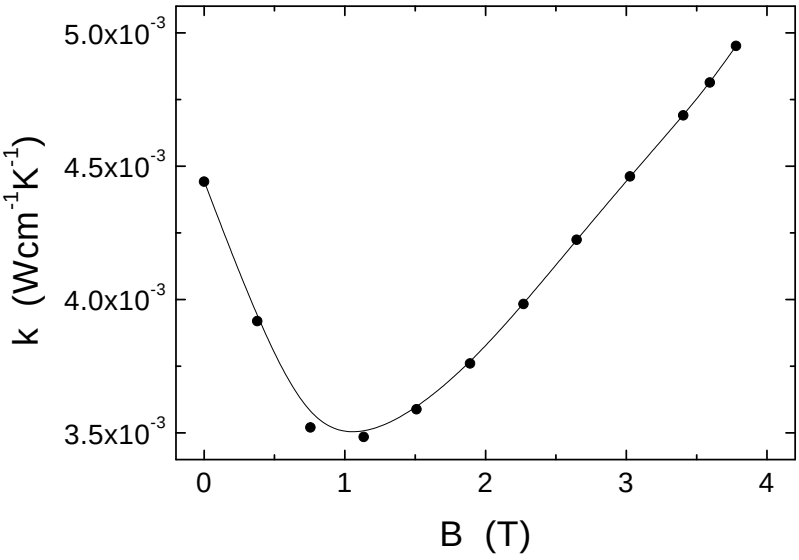

Figure 4.3: *The thermal conductivity of TGG 2 as a function of magnetic field at 6 K. The data is not corrected for the change of the mean sample temperature. The solid line is only meant to guide the eye. We only show data for positive field values.* k_{xx} *is necessarily of even symmetry with respect to* B*.*

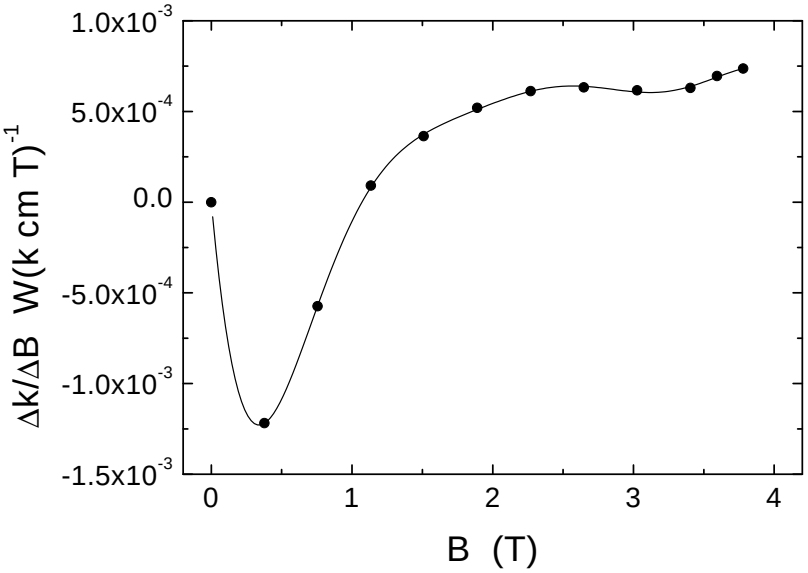

Figure 4.4: *Derivative of the thermal conductivity with respect to the magnetic field. The solid line is only meant to guide the eye.*

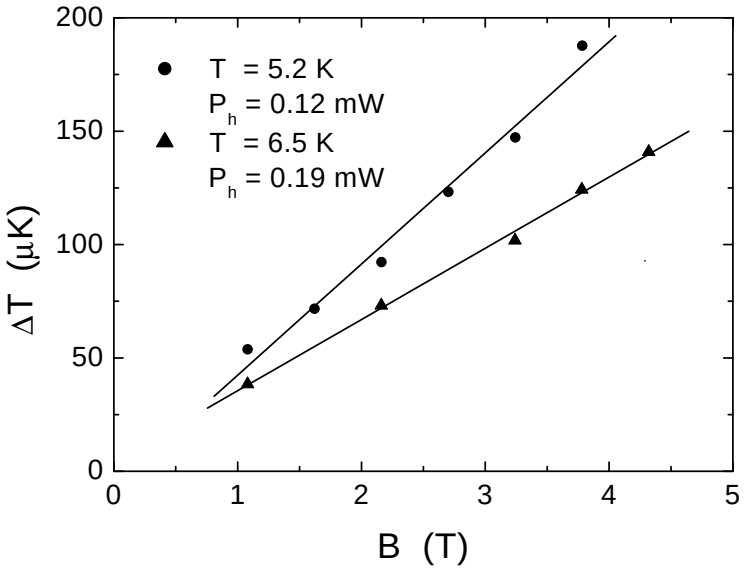

Figure 4.5: *The magneto-transverse temperature difference of TGG 1 as a function of magnetic field for different heater powers and temperatures. The straight lines are linear fits to the data.*

.

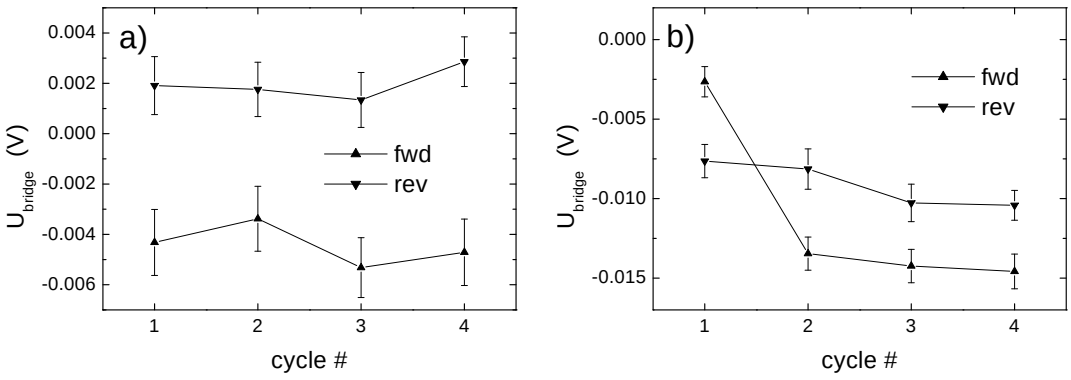

Figure 4.6: *Cycle measurements. a) The respective values for positive and negative field directions vary only within the error bars due to global temperature fluctuations. b) measurement in which the first data point is distinct from the other points for the same field direction.*

Figure 4.7 shows the results obtained on sample TGG 2. Measurements for different heater powers were performed at constant mean sample temperature (in zero field) in order to verify the linear dependence on j. The linear dependence on j is shown in figure 4.8 where the slopes of figure 4.7 are plotted as a function of the applied heater power at the sample heater. A further important experiment is the measurement of the dependence of the magneto-transverse temperature difference on the relative orientation of j and B. As the effect is proportional to $B \cdot j$ it must vanish for $B \| j$. Figure 4.9 shows data for $B \| j$ and $B \perp j$. The measurements presented above fulfill a number of necessary conditions, that are characteristic for the magneto-transverse thermal conductivity of dielectric solid which we are looking for. Namely:

- The effect is odd in the magnetic field and linear in B for low fields.
- The effect is linear in j.
- The effect vanishes for $B \| j$.

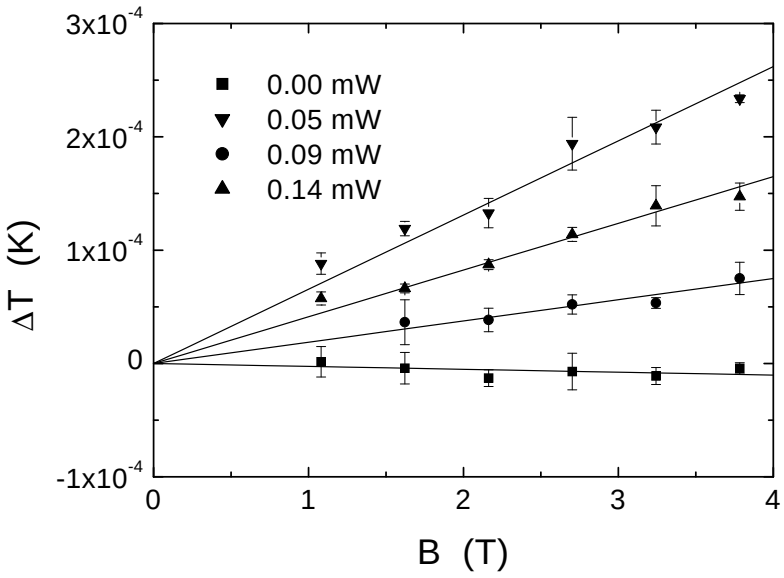

Figure 4.7: *The magneto-transverse temperature difference of TGG 2 as a function of magnetic field for different heater powers. The mean sample temperature was adjusted to 5.45 K in zero field for all curves. The data is not corrected for the change of the mean sample temperature due to the B-dependence of k_{xx}. The straight lines are linear fits to the data.*

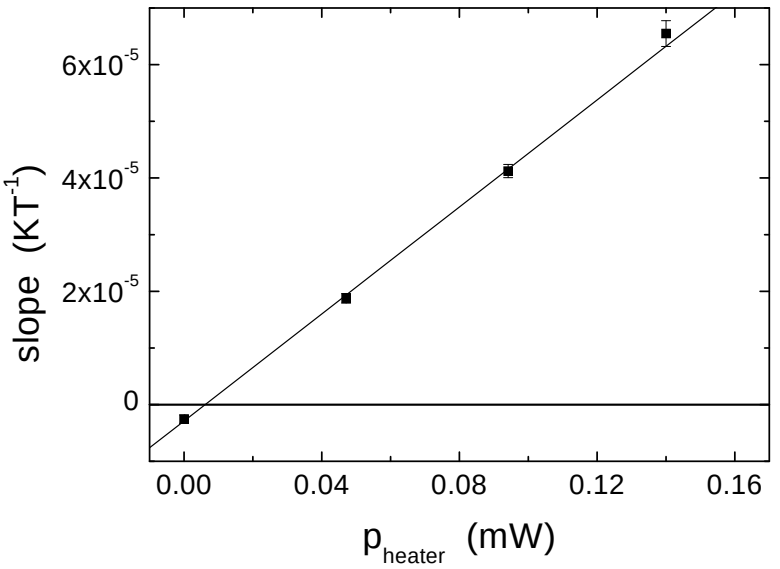

Figure 4.8: *The magneto-transverse temperature difference normalized to the magnetic field (slope of the linear fits in figure 4.7) as a function of heater power. The mean sample temperature was adjusted to 5.45 K in zero field for all curves. The straight line is a linear fit to the data.*

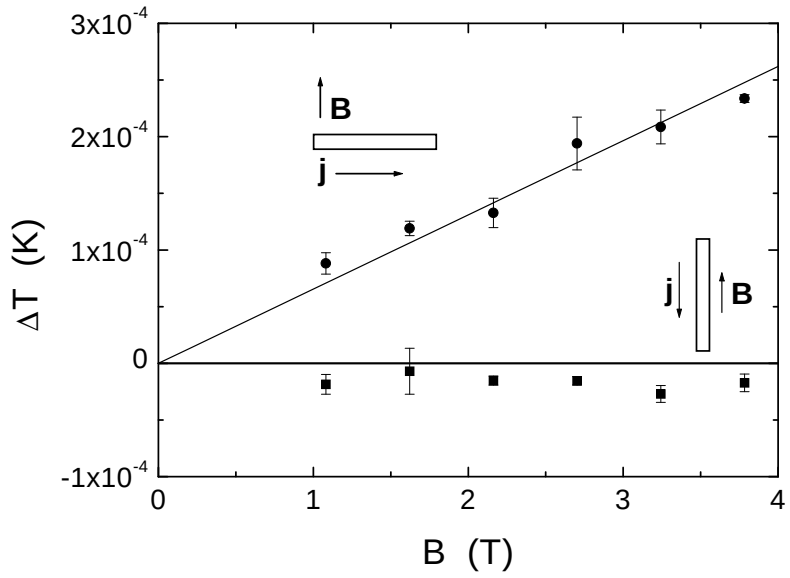

Figure 4.9: *The field normalized magneto-transverse temperature difference for heat currents perpendicular (circles) and parallel (squares) to the field. The mean sample temperature was adjusted to 5.45 K in zero field for all curves.*

4.5 Significance of the results

In this section we show that the data set presented above allows to rule out trivial artifacts like effects of the magnetic field on electronic instruments. In the section on the measurement principle we discussed the fact that the measurement critically relies on the field and temperature stability. The relations derived there will now be used in order to put the data presented above to a test.

Effect of the magnetic field on the electronics

Part of the electronic instruments is very close to the magnet for technical reasons. One could argue, that the detection of a transverse temperature difference results from effects of odd symmetry in B in the electronics subject to the stray field of the magnet. But this kind of artifact can easily be excluded by the measurements of characteristic dependencies in which the transverse temperature difference is scaled to zero despite the presence of a magnetic field:

- The dependence on the originating heat current j. For a given field strength the magneto-transverse temperature difference scales linearly with j and vanishes for $j = 0$. Figure 4.8.
- The angle dependence. The magneto-transverse temperature difference vanishes for $j||B$ with $j \neq 0$ and $B \neq 0$. Figure 4.9.

Type 1: Temperature drift(+ different sensitivity to temperature)

A global temperature change of ΔT while reversing the field leads to the detection of an apparent temperature difference $\Delta T_{\perp}^{ev}$ of:

$$\Delta T_{\perp}^{ev} = -\frac{s_1 - s_2}{s_m}\Delta T \tag{4.2}$$

With the following parameters:

parameter	symbol	value
sensitivity difference	$s_1 - s_2$	6 Ω/K
mean sensitivity	s_{mean}	-200 Ω/K
temperature drift	ΔT	$5 \cdot 10^{-4}$ K

The estimate of $5 \cdot 10^{-4} K$ for the temperature drift is conservative. This artifact shows no characteristic dependence and can easily be ruled out by measuring more than on cycle. In fig. 4.10 we show the apparent temperature difference together with typical data.

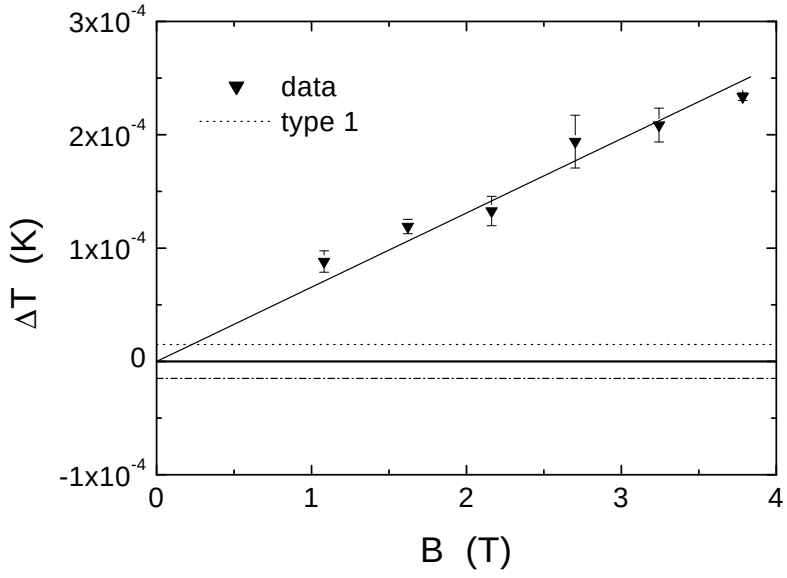

Figure 4.10: *The magneto-transverse temperature difference (down triangles) together with an estimate for an artifact of type 1. It can either be of positive (dashed line) or negative sign (dash-dotted line).*

Type 2: Field imprecision (+ different sensitivity to temperature)

A hysteresis in B means different longitudinal thermal conductivity at positive and negative field and thus to a different gradient along the sample. The thermometers R_1 and R_2 that are at position d from the anchoring point are therefore at different temperatures for positive and negative field. We showed that this leads to the detection of an apparent transverse temperature difference of:

$$\Delta T_{\perp}^{ev} = \frac{jd}{k_{xx}(B,T)^2} \frac{\partial k_{xx}(B,T)}{\partial B} \Delta B \frac{s_1 - s_2}{s_m} \tag{4.3}$$

With the following parameters:

parameter	symbol	value
heat current	j	$3.14 \cdot 10^{-3}$ W/cm^2
thermometer position	d	4.47 mm
field hysteresis	ΔB	0.02 T
thermal conductivity	k_{xx}	figure 4.3
derivative	$\partial k_{xx}/\partial B$	figure 4.4
sensitivity difference	$s_1 - s_2$	6 Ω/K
mean sensitivity	s_{mean}	-200 Ω/K

In fig. 4.11 we show the apparent temperature difference together with typical data. This artifact has a characteristic field dependence due to k_{xx} and $\partial k_{xx}/\partial B$. It is small for high fields.

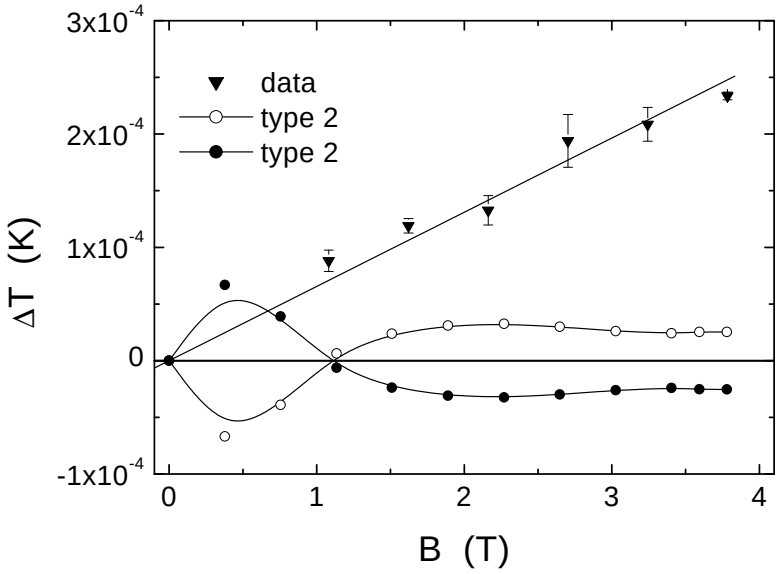

Figure 4.11: *The magneto-transverse temperature difference (down triangles) together with an estimate for an artifact of type 2. It can either be of positive (full circles) or negative sign (open circles).*

Type 3: Field imprecision (+ different magnetoresistance)

A magnet hysteresis of ΔB leads to the detection of an apparent transverse temperature difference $\Delta T_{\perp}^{ev}$:

$$\Delta T_{\perp}^{ev} = -\frac{s_1^m - s_2^m}{s_m}\Delta B \tag{4.4}$$

With the following parameters:

parameter	symbol	value
sensitivity difference	$s_1^m - s_2^m$	figure 3.7
mean sensitivity	s_{mean}	$-200\ \Omega/\mathrm{K}$
field hysteresis	ΔB	0.02 T

In fig. 4.12 we show the apparent temperature difference together with typical data. This artifact has a characteristic field dependence because s_1^m and s_2^m depend on B. It is negligible compared with the other contributions.

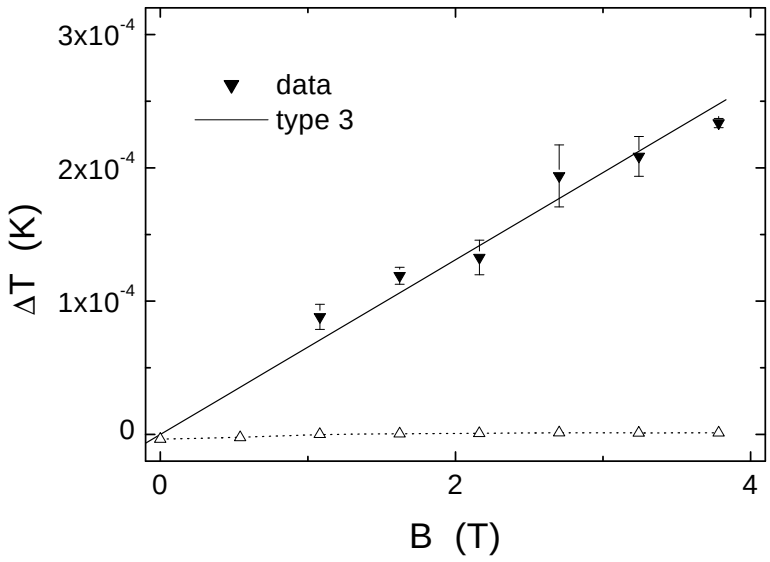

Figure 4.12: *The magneto-transverse temperature difference (down triangles) together with an estimate for an artifact of type 3. It can either be of positive or negative sign. For clarity we only show the positive sign (open triangles).*

Type 4: Field imprecision (+ misalignment of the thermometers)

A misalignment δ of the thermometers R_1 and R_2 leads to the detection of an apparent transverse temperature difference of:

$$\Delta T_{\perp}^{ev} = \frac{j\delta}{k_{xx}(B,T)^2} \frac{\partial k_{xx}(B,T)}{\partial B} \Delta B \tag{4.5}$$

With the following parameters:

parameter	symbol	value
heat current	j	$3.14 \cdot 10^{-3}$ W/cm^2
thermometer misalignment	δ	0.22 mm
field hysteresis	ΔB	0.02 T
thermal conductivity	k_{xx}	figure 4.3
derivative	$\partial k_{xx}/\partial B$	figure 4.4

This contribution has the same characteristic dependence on B as the field imprecision together with different sensitivities of R_1 and R_2. The relative sign and size is given by:

$$\frac{d}{\delta} \frac{s_1 - s_2}{s_m} \tag{4.6}$$

For the data presented here for sample TGG 2 this parameter is of the order of 0.6. In fig. 4.13 we show the apparent temperature difference together with typical data.

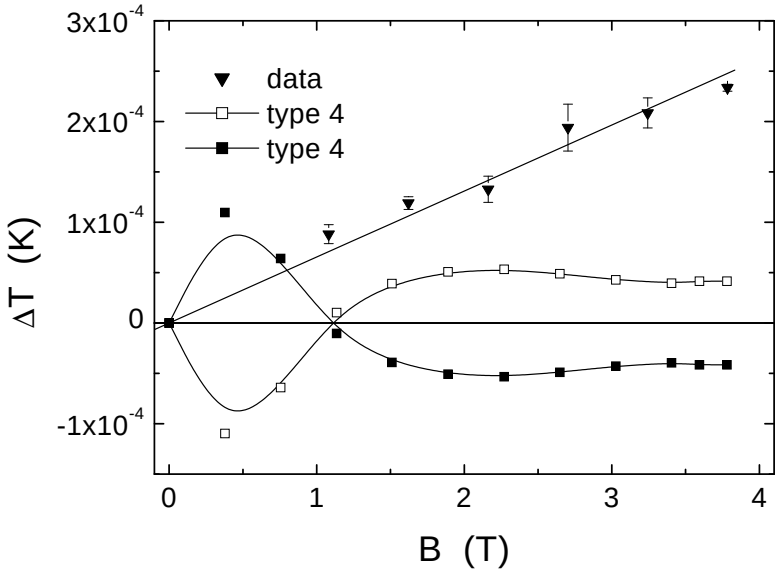

Figure 4.13: *The magneto-transverse temperature difference (down triangles) together with an estimate for an artifact of type 4. It can either be of positive (full squares) or negative sign (open squares).*

4.6 Conclusion

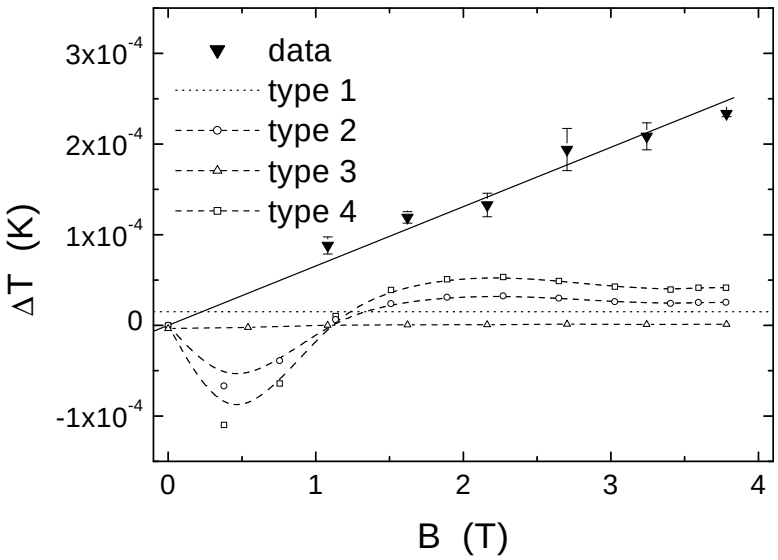

Figure 4.14: *The different types of possible artifacts together with typical data.*

In fig. 4.14 we show the four possible artifacts analyzed above together with a typical data set. Type 1 is ruled out by measuring at least 3 full cycles for every final data point, it is naturally very small and does not depend on B. Type 3 is negligible, compared with the other contributions. Type 2 and type 4 have the same characteristic dependence on B and may or may not cancel out partially depending on their relative sign. They are important at fields below 1 T where no data for the transverse temperature difference is available and can be considered as a constant at higher fields. They scale linearly with j and therefore have always the same relative size with respect to the data. Type 2 and type 4 can neither account for the linear dependence of the data on the magnetic field nor for the fact that the transverse temperature difference is vanishing for $j||B$. We further ruled out effects of the magnetic field on the instruments used in the measurements. A point of serious concern are the jumps observed in a number of measurements on the sample TGG 2. To our knowledge, the data and dependencies presented in this thesis could not be explained by some - not yet understood- effect that occasionally shows up in these jumps. The best argument against this objection are again measurements in which the magneto-transverse effect is scaled to zero. In some of these, the jumps have also been observed. Magnetic phase transitions could be at the origin of such phenomena but can be excluded for temperatures above 0.6 K [Sla71].

The data is therefore considered to be significant.

Due to the lack of reliable simultaneous measurements of k_{xy} and k_{xx} we always presented the transverse temperature difference ΔT instead of k_{xy}, but we are able to give indicative values: At mean sample temperatures around 6 K and zero field thermal

conductivities of $4.5 \cdot 10^{-3}$ $\mathrm{WK^{-1}cm^{-1}}$, the magneto-transverse thermal conductivity is approximately $5 \cdot 10^{-7}$ $\mathrm{WK^{-1}cm^{-1}T^{-1}}$. The Hall angle is about $\alpha = 1.6 \cdot 10^{-4}$ rad $\mathrm{T^{-1}}$.

Chapter 5

Summary / Zusammenfassung

5.1 English summary

In analogy with Ohm's law for the electrical conductivity, diffusive transport of heat can be described by a linear relation between the resulting heat current and the original gradient. In 1931 Onsager showed, that the thermal conductivity tensor may contain an antisymmetric contribution, induced by a magnetic field. This leads to a heat current perpendicular to both, the original gradient and the applied magnetic field. In a confined sample geometry, this transverse current is balanced by a transverse temperature difference. in metals the corresponding effect has been known for a long time: The Righi-Leduc-effect is caused by the electronic contribution to the thermal conductivity. Later, a magneto-transverse thermal conductivity of paramagnetic molecular gases, the so called Senftleben-Beenakker-effect was observed. The effect is due to an anisotropic scattering cross-section of the diffusing gas molecules responsible for the conduction of heat.

As there is no net charge associated with phonons no such effect has been expected for the phonon thermal conductivity. But phonons describe the collective motion of particles carrying charge and spin and are thus influenced by a magnetic field. The observation of the magneto-transverse diffusion of light gives a clue on how such an effect might be realized in the diffusion of classical waves.

To our knowledge there is no investigation of the magneto-transverse thermal conductivity reported in the scientific literature. In the diploma-thesis of the author, we investigated this new effect in diamagnetic samples, however without an unambiguous observation of the effect.

In this thesis we investigated the effect in paramagnetic materials in which large effects are expected due to the resonant scattering of phonons.

In the theoretical introduction we argue, that an antisymmetric contribution to the thermal conductivity tensor is thermodynamically allowed, using Onsagers relations for diffusive transport. We show that this contribution will lead to a transverse temperature difference in confined sample geometries. Today there is no theory on a microscopic realization of the effect. We therefore recur on a comparison of phonon sand photons. After a review of the results of Rikken and Tiggelen for the optical case

we therefore worked out the analogies between photons and phonons and presented useful relations for the choice of samples and the understanding of the experiments.

In the experimental part we presented the techniques for the measurement of the thermal conductivity as a function of temperature and magnetic field. We specially focused on the setup for the measurement of the magneto-transverse thermal conductivity with ultra high resolution. we analyzed the setup and the protocols to identify possible artifacts.

All measurements presented in this thesis have been performed on samples of $Tb_3Ga_5O_{12}$. The sample has been specified by measuring the longitudinal thermal conductivity as function of temperature and magnetic field. The analysis of the low temperature part of the thermal conductivity shows that scattering mean free path is dominated by scattering at point defects and by resonant scattering. From the magnetic field dependence of the thermal conductivity on can conclude on a strong spin phonon coupling which makes the material suitable for an investigation of the magneto-transverse thermal conductivity.

We present a complete data set fulfilling all criteria for a phenomenological observation of the effect. A detailed analysis of possible artifacts supports the significance of the data.

5.2 Deutsche Zusammenfassung

Diffusiver Transport von Wärme kann analog zum Ohmschen Gesetz der elektrische Leitfähigkeit durch eine lineare Relation zwischen dem resultierenden Wärmestrom und dem ursächlichen Temperaturgradienten beschrieben werden. Onsager zeigte 1931 aufgrund thermodynamischer Betrachtungen, dass der Leitfähigkeitstensor eine magnetfeldinduzierten antisymmetrischen Beitrag haben kann. Dies führt zu einem Wärmestrom senkrecht zu beidem, dem ursprünglichen Gradienten und dem externen Magnetfeld. In einer begrenzten Probengeometrie wird dieser transversale Wärmestrom durch ein transversale Temperaturdifferenz ausgelichen. In Metallen ist dieser Effekt schon seit langem bekannt: Der Righi-Leduc-Effekt wird durch den elektronischen Beitrag zur thermischen Leitfähigkeit verursacht. Später wurde weiter eine magneto-transversale Wärmeleitfähigkeit in molekularen, paramagnetischen Gasen entdeckt: Der Beenakker-Senftleben-Effekt beruht auf einem anisotropen Streuquerschnitt in der Diffusion der Gasmoleküle.

Da Phononen keine Ladung tragen, wurde bisher angenommen, ein analoger Effekt in der phononischen Leitfähigkeit könne nicht existieren. Phononen beschreiben jedoch die kollektive Bewegung von Teilchen, die Ladung und Spin tragen. Die Beobachtung der magnetotransversalen Diffusion von Licht gibt neue Hinweise auf die Realisierung solcher Effekte in der Diffusion klassischer Wellen.

In der wissenschaftlichen Fachliteratur findet sich unseres Wissens keine Behandlung des magneto-transversalen transports von Phononen. In der Diplomarbeit des Autors wurde dieser neuen Effektes erstmalig in diamagnetischen Materialien untersucht. Es gelang jedoch kein eindeutiger Nachweis.

Die vorliegende Doktorarbeit beschäftigt sich erneut mit dem Nachweis dieses Effektes. Nach einer Erweiterung und Verfeinerung der Methoden wurden Messungen an paramagnetischen Materialien durchgeführt, für die aufgrund resonanter Phononenstreuung grosse Effekte erwartet werden.

In einer theoretischen Einührung wird zunächst unter Rückgriff auf die Onsager-Relationen für den diffusiven Transport argumentiert, dass ein antisymmetrischer Beitrag zum Wärmeleitfähigkeitstensor thermodynamisch erlaubt ist. Wir zeigen, dass dieser Beitrag in einer begrentzten Probengeometrie zum Auftritt einer magneto-transversalen Temperaturdifferenz führt. Es gibt jedoch bislang keine Theorie zu einer mikroskopischen Realisierung des Effektes. Wir greifen deshalb auf einen Vergleich zwischen Phononen und Photonen zurück. Nach einer Zusammenfassung der Hauptresultate von Rikken und Tiggelen für den optischen Fall entwickeln wir Analogien zwischen Photonen und Phononen und führen für die Probenauswahl und das Verständnis der Experimente nützliche Relationen ein.

Im experimentellen Teil stellen wir die Techniken zur Messung der Wärmeleitfähigkeit als Funktion von Temperatur und Magnetfeld vor. Besonderes Augenmerk gilt der Dikussion der Apparatur zur hochpräzisen Messung der magneto-transversalen Wärmeleitfähigkeit, die in dieser Doktorarbeit entwickelt wurde. In einer Analyse der Apparatur und der verwendeten Protokolle identifizieren wir mögliche Artefakte.

Alle hier präsentierten Messung wurden an $Tb_3Ga_5O_{12}$ durchgeführt. Die Probe wurde zunächst durch Messungen der Wärmeleitfähigkeit als Funktion der Temperatur spezifiziert. Eine Analyse des Tieftemperaturverhaltens der Wärmeleitfähigkeit lässt den Schluss zu, dass dass die mittlere freie Weglänge durch Streuung an Punktdefekten und durch resonante Streuung dominiert ist. Die Magnetfeldabhangikeit der longitudinalen Wärmeleitfähikeit lässt auf eine starke Spin-Phononen Kopplung schliessen, wodurch sich das Material als günstiger Kandidat für einen Nachweis der magneto-transversalen Wärmeleitfähigkeit erweist.

Wir präsentieren einen vollständigen Datensatz der alle Kriterien für einen phänomenologischen Nachweis des Effektes erfüllt. Wir untermauern die Signifikanz der Daten durch eine detaillierte Analyse und den Ausschluss einer grossen Zahl an Artefakten.

Bibliography

[Str00] This thesis is the logical evolution of the author's diploma thesis "Phonon transport in magnetic fields". The diploma thesis was extensively cited. Citations of this diploma thesis are not indicated explicitly. 6, 15, 16

[Ana72] Anastassakis E., Burnstein E., Maradudin A. A., Minnick R. Morphic effects-III. Effects of an external magnetic field on the long wavelength optical phonons. J. Phys. Chem. Sol. **33** 519 (1972) 14

[Ana81] Anderson A. C. The Kapitza thermal boundary resistance between two solids. In: Nonequilibrium superconductivity, Phonons and Kapitza Boundaries. Nato advanced study institutes series B **65** 1 ISBN 0-306-40720-5 (1981) 36

[Cal58] Callaway J. Model for lattice thermal conductivity at low temperatures. Phys. Rev. **113** 1046 (1958) 20

[Cas45] Casimir H. B. G. On Onsager's principle of microscopic reversibility. Rev. mod. Phys. **17** 343 (1945) 7

[Che76] Cheeke J. D. N., Ettinger H., Hebral B. Analysis of heat transfer between solids at low temperatures. Can. J. Phys. **54** 1749 (1976) 36

[Düc00] Düchs G. Photonic Hall effect of inactive Mie scatterers in a Faraday active matrix. Phys. Rev. E. **62**(2) 2840 (2000) 12

[Etc96] Etchegoin P., Phillips R. T. Photon focusing, internal diffraction and surface states in periodic dielectric structures. Phys. Rev. B. **53** 12 674 (1996) 11

[Fle76] Fletcher R. The high field galvano- and thermomagnetic effects in cadmium. J. L. Temp. Phys. **22** 39 (1976) 31

[Gui85] Guillot M., Marchand A., Nekvasil V., Tcheou F. Step-like magnetisation curves in $Tb_3Ga_5O_{12}$. J. Phys. C **18** 3547 (1985) 46, 47

[Hak79] Hardy J. R., Karo A. M. The lattice dynamics and statics of the alkali halide crystals. Plenum Press. ISBN 0-306-40221 (1979) 15

[Hal79] Hall E. On a new action of the magnet on electrical currents. Am. J. Math. **2** 287 (1879) 5

[Haw70] Harrington J. A., Walker C. T. Phonon scattering by point defects in CaF_2, SrF_2, BaF_2. Phys. Rev. B **1** 882 (1970) 20

[Her67] Hermans L. J. F., Fortuin P. H., Knaap H. F. P., Beenakker J. J. M. Transverse heat transport in polyatomic gases under influence of a magnetic field. Phys. Lett. **25 A** 81 (1967) 5

[Hof01] Hofmann M. et al. Strong damping of phononic heat current by magnetic excitations in $SrCu_2(BO_3)_2$ Phys. Rev. Lett. **87**(4) 047202 1-4. 19

[Kle66] Klein M. V., Caldwell R. F. Low temperature system for thermal conductivity measurements. Rev. Sci. Instr. **37** 1291 (1966) 28

[Kle55] Klemens P. G. The scattering of low frequency lattice waves by static imperfections. Proc. Phys. Soc. (London) **A68** 1113 (1955) 17, 22

[Led87] Leduc M. A. Sur la conductibilité calorifique du bismuth dans un champ magnétique et la déviation des lignes isothermes. J. de Phys. 2^e serie **6** 373 (1887) 5

[Nee72] Neelmani, Verma G. S. Phonon conductivity of trivalent rare-earth-doped Gallium and Aluminium Garnets. Phys. Rev. B. **6** 3509 (1972) 19, 46

[On31-1] Onsager L. Reciprocal relations in irreversible processes I Phys. Rev. **37** 405 (1931) 7

[On31-2] Onsager L. Reciprocal relations in irreversible processes II Phys. Rev. **38** 2265 (1931) 7

[Rig87] Righi A. Atti Accad. Lincei **3 (1)** 481 (1887) This reference figures for completness only. The paper was not available to the author.

[Rik96] Rikken G. L. J. A., Tiggelen, B. A. Observation of magnetically induced transverse diffusion of light. Nature **381** 54 (1996) 5, 12

[Rik96-2] Rikken G. L. J. A. Calculation of the acoustic Verdet constant for the propagation of transverse waves in NaCl-structures along directions of high symmetry. (private communication)(1996) 15

[Rik97] Rikken G. L. J. A., Sparenberg A., van Tiggelen B. Der Photonen Hall Effekt. Phys. Bl. **53** 133 (1997) 12, 13

[Rik01] Rikken G. L. J. A., Folling J., Wyder P. Electrical magnetochiral anisotropy. Phys. Rev. Lett. **87** 23 (2001) 8

[Rou70] Roundy V., Mills d. L. Thermal conductivity of paramagnetic salts at low temperatures. Phys. Rev. B **1** 3703 (1970) 19

[Sla57] Slack G. A. Thermal conductivity of potassium chloride crystals containing calcium. Phys. Rev. **105** 832 (1957) 28

[Sla71] Slack G. A., Oliver D. W. Thermal conductivity of garnets and phonon scattering by rare earth ions. Phys. Rev. B **4** 592 (1971) 45, 46, 47, 58

[Swa88] Swartz E. T. Cooling the sample. in Richardson R. C., Smith E. N. Experimental techniques in condensed matter physics at low temperatures. 154 Addison-Wesley ISBN 0-201-15002-6 36

[Tig95] van Tiggelen B. A. Transverse diffusion of light in Faraday-active media. Phys. Rev. Lett. **75** 422 (1995) 11

[Tou76] Touloukian Y. S., Powell R. W., Ho C.Y., Klemens P. G. Thermophysical Properties of Matter **2** Thermal conductivity. Nonmetallic solids. IFI / Plenum NewYork - Washington ISBN 306-67022-4 (1976) 28

[Tuc80] Tucker J. W. Theory of the acoustic Faraday and Cotton-Mouton effects in Ni^{2+}-doped $KMgF_3$. J. Phys. C **13** 1767 (1980) 6, 19, 20

[Vin85] Vineyard G. H. Effect of a magnetic field on the vibrations of an ionic lattice. Phys. Rev. B **31** 814 (1985) 6, 14, 15, 16

[Wei95] Weis O. Differential and total scattering cross-section for phonon beams with special application to scattering by isotopes. Z. Phys. B. **96** 525 (1995) 17, 18

Acknowledgements

A thesis is never an achievement of the thesis student alone. The whole laboratory contributes directly or indirectly with it's infrastructure, environment and collective knowledge. Its a pleasure to thank all the people who made this work possible.

- Many thanks to Professor Wyder for giving me the opportunity to prepare my thesis in this exceptional laboratory. And many thanks for his enduring support of this project.
- Great thanks to Geert Rikken for sharing his fascinating ideas and for teaching me on how to steal nature's secrets. It was a pleasure to work with you!
- I would like to acknowledge Professor Schatz and Professor Dehnen from the University of Konstanz for participating in the jury.
- Louis Jansen and Nico Gauss made the very first attempts in detecting the magneto-transverse phonon transport and helped me a lot on my first steps in this project and in this laboratory, a long time ago.
- Many things wouldn't have worked without the valuable help of Peter van der Linden.
- I am grateful to Hans Dresler for projecting my ideas into drawings and to Claude Mollard, Robert Pankow and Jürgen Spitznagel for materializing drawings into sample holders and experiments.
- Thanks to Sebastien Buisson, Vinh Tran and Henk Jongbloeds for keeping my computer and the software on it running.
- I want to thank Ursula Laitenberger, Brigitte Indigo, Ingrid Girardet-Beyer and Gislaine Meneroud for keeping administration far from my thesis and for much more.
- This thesis would have been much less interesting, productive and enjoyable without the lab-mates: Georg, Clemens, Ekkehard, Eckhard, Thomas, Ede, Roman, Roland, Markus, Andreas, Jörg, David and Ilya. Thank you very much.